Computational Study of Cell Mobility and Transport Phenomena Through Textile Vascular Grafts Using a Multi-Scale Approach

Dissertation

by

Raúl A. Valencia

Advisors: Manuel García, Ph.D.

and John Bustamante, M.D., Ph.D.

EAFIT UNIVERSITY

Doctoral Program in Engineering

Dedication

I dedicate this work to my loving family for being patient throughout the process and for keeping their prayers and hope alive.

Acknowledgments

I would like to thank my advisors Dr. Manuel Garcia (EAFIT) and M.D., Ph.D. John Bustamante (UPB) for their guidance and encouragement. I would also like to thank Professor Yusheng Feng and Dr. Sarah Boukhris for the opportunity to work with their team at UTSA, to fellow graduate students from the Applied Mechanics research group (EAFIT) for their conversations and collaboration with Numerical Methods, to Dr. Lina Hoyos, to Dr. Isabel Cristina Ortiz and to fellow graduate student Yulieth Montoya (UPB), for their collaboration and advice on experimental tests, to Camilo Andrés Páramo for his collaboration on random mat CAD models and to Mauricio Arroyave (EAFIT) for his collaboration on SEM micrographs.

Abstract

Textile vascular grafts are biomedical devices that serve as partial replacement of damaged arterial vessels, prevent aneurysms rupture and restore normal blood flow. It is believed that the success of a textile vascular graft, in the healing process after implantation, is due to the porous micro-structure of the wall. Among the key properties that take part in the tissue repair process are the type of fabric and degree of porosity and permeability, defining the ability of a well-controlled environment for the neovascularization, nutrient supply, and cellular transport. Although the transport of fluids through textiles is of great technical interest in biomedical applications, little is known about predicting the micro-flow pattern and the transport and deposition of individual platelets, related with the graft occlusion. Often, this information is difficult to obtain experimentally both *in vivo* and *in vitro*, representing a great deal of research efforts.

The aim of this work is to investigate how the type of fabric, permeability and porosity affect both the local fluid dynamics at several scales and the fluid-particle interaction among platelets in textile grafts with an anastomosis of end-to-end configuration. Two types of samples were analyzed: woven and electrospun, this last one has been manufactured. This study involves both experimental and computational tests. The experimental tests were performed to characterize the permeability and porosity under static conditions. The computational tests are based on a multi-scale approach where the fluid flow was solved with the Finite Element Method and the discrete particles were solved with the Molecular Dynamic Method. The fluid-particle interaction was accomplished in one-, two-, and four-ways, where the blood was considered as a suspension of platelets in plasma. The textile wall was considered as a porous media with two scales of length: straight tubular structure with porous walls for the macro-domain and representative unit cells of fabric for the micro-domain. Additionally, it presents the implementation of a numerical case that includes one of the main applications of textile vascular grafts to repair Abdominal Aortic Aneurysms (AAA).

The results have shown that the type of fabric in textile vascular grafts and the degree of porosity and permeability affect the local fluid dynamics and the level of penetration of platelet particles through the graft wall at several length scales, thus indicating their importance as design parameters. It was found that the permeability is strongly depends on the micro-structure of the fabric, changing the local fluid dynamics and the time of residence of platelets inside the wall. Moreover, the porous walls cause deviations from Poiseuille flow due to leakage flow through the wall from a

macroscopic viewpoint. Lastly, it was possible to observe that the textile wall with different porosities, acting like a barrier between the blood and an aneurysmal zone, affects the flow pattern, the number of platelets adhered to the artificial surface and the time of residence of platelets into the aneurysmal zone.

In conclusion, predicting the flow pattern and the mobility of blood cells through the textile wall before the graft is manufactured, the development of new textile grafts can be improved.

Keywords: textile vascular grafts, porous media, local fluid dynamics, fluid-particle interaction, multi-scale approach.

Publications and Other Scientific Communications

- Valencia, R., García, M. and Bustamante, J. Fluid Structure interaction in the optimization of textiles vascular implants. In Proceedings of 10th World Congress On Computational Mechanics (WCCM 2012). Sao Paulo, Brasil, Jul. 2012.

- Valencia, R., García, M. and Bustamante, J. Cell migration and mass transport simulation through vascular graft (porous media) using a Multi-Scale Approach. In Proceedings of IX CONGRESO COLOMBIANO DE METODOS NUMERICOS: Simulación en Ciencias y Aplicaciones Industriales. IX CCMN 2013. Cali, Colombia, Aug, 2013.

- Broukris, S., Valencia, R. and Feng, Y. Tumor Cell Migration And Nanoparticle Transport Simulation Using A Multi-Scale Approach. In Proceedings of BMES Annual Meeting. Biomedical Engineering Society (BMES) 2013. Seattle, Washington, Sep, 2013.

- Niño, M, Fernadez, A. and Valencia, R. Caracterización y propiedades en implantes textiles vasculares. Undergraduate thesis. UPB. 2013

- Broukris, S., Valencia, R. and Feng, Y. Mathematical modeling and experimental validation of cancer cell migration in a three-dimensional tumor matrix. In Proceedings of 11th World Congress On Computational Mechanics (WCCM 2014). Barcelona, Spain, Jul. 2014.

- Valencia, R., García, M. and Bustamante, J. Textiles en aplicaciones vasculares. Poster presentation at Colombiatex expo. Medellín, Colombia, 2015.

- Valencia, R., García, M. and Bustamante, J. Modelling of a Textile Vascular Graft in an Aneurysm with Clot Formation using a Multi-Scale Approach. In Proceedings of X CONGRESO COLOMBIANO DE METODOS NUMERICOS: Simulación en Ciencias y Aplicaciones Industriales. X CCMN 2015. Cartagena, Colombia, Sept, 2015.

- Sanchez, S, and Valencia, R. Efecto del espesor y la deposición celular sobre la permeabilidad y porosidad en membranas electrohiladas para implantes vasculares. Undergraduate thesis. UPB. 2015

- Valencia, R., García, M. and Bustamante, J. Cell migration and mass transport simulation through vascular graft (porous media) using a Multi-Scale Approach. In Proceedings of 11th World Congress On Computational Mechanics (WCCM 2014). Barcelona, Spain, Jul. 2014.

- Feng, Y., and Boukhris, S. , Ranjan, R. and Valencia, R. Biological Systems: Multiscale Modeling Based on Mixture Theory, Chapter 11: Page 257-286, Multiscale Modeling in Biomechanics and Mechanobiology, Suvranu De (Eds), Springer-Verlag, London, DOI 10.1007/978-1-4471-6599-6_11, © 2015.

- Analysis of the Type of Fabric, Blood Flow and Cellular Interaction in Textile Vascular Grafts: a Multi-Scale Approach. Submited article to The Journal of the Textile Institute (United Kingdom).

- Modelling of a Textile Vascular Graft in an Aneurysm with Clot Formation using a Multi-Scale Approach. Article in preparation.

Nomenclature

Abbreviations

AAA	Abdominal Aortic Aneurysm
PRI	Particle Residence Index
FDA	Food Drug Administration
SEM	Scanning Electron Microscope
MRA	Magnetic Resonance Angiography
FE	Finite Element method
MD	Molecular Dynamic
RUC	Representative Unit Cell
PIV	Particle Image Velocimetry
FV	Finite Volume method
WSS	Wall shear stress

Symbols

Re	-	Reynolds number
Re_p	-	particle Reynolds number
ε	-	porosity
k	m^2	permeability
K	m/s	hydraulic conductivity
$\mathbf{u}$	m/s	velocity
p	kg/m$\cdot s^2$	pressure
ρ	kg/m^3	density
μ	kg/(m$\cdot$s)	dynamic viscosity
d_p	$\mu\mathrm{m} = 10^{-6}\mathrm{m}$	diameter of the particle
m_p	kg	mass of the particle
$\mathbf{v}_p$	m/s	velocity of the particle
τ_p	s	particle relaxation time
x, y, z	-	Cartesian coordinates

k_{ad}	N/m	constant proportional to adhesion force
k_{ag}	N/m	constant proportional to aggregation force
d_{ad}	m	distance of adhesion
d_{ag}	m	distance of aggregation
r_o	m	length among particles without overlapping
$\mathbf{n}_{ij}$	-	vector between the platelet particles i and j
$\frac{\mathbf{u}}{\varepsilon}$	m/s	interstitial velocity
F	kg·m/s^2	force acting on a single particle
g	m/s^2	gravity
C_D	-	drag coefficient
t	s	time
τ	kg/m·s^2	shear stress

Contents

List of Figures

List of Tables

Chapter 1

INTRODUCTION

1.1 Textiles as Vascular Grafts

Atherosclerosis accounts for almost one half of all deaths in Europe [23] and each year, 1.4 million patients in the USA need vascular prostheses [47]. Vascular grafts play an important role that serve as a solution for the partial replacement or bypass of damaged arterial vessels, to prevent hemorrhage from arteries (e.g, aneurysms), to overcome obstructions in the aorta or other major arteries, as well as for vascular access (renal dyalisis) [87, p.45].

These biomedical textiles have been used clinically since the 1950s[14]. Indeed, the first textile vascular prosthesis was implanted in humans to replace an Abdominal Aortic Aneurysm(AAA) in 1954 by Drs. Voorhees and Blakemore at the Columbia Presbyterian Hospital in New York [62]. The patient died 30 minutes after the operation, but it was the beginning of the research of textile vascular grafts.

Ideally, the graft should have characteristics similar to a healthy vessel. Some important features required by the Food and Drug Administration (FDA) [36] are: non-thrombogenic surface, proven high patency, ability to generate vascularized tissue, among others [16, 56].

Straight and bifurcated fabric grafts are available in a wide variety of sizes and shapes, ranging from 4 to 35 mm in diameter [87, p.56]. The options which are currently available for these transplants are biological grafts and synthetic grafts with biomedical textiles. Biological grafts are the preferred materials to reconstruct vascular segments, but their use is limited due to the lack of tissue donors, patients with previous interventions or anatomical variability. For that reason, synthetic grafts are widely used [16]. The most commonly used materials in synthetic grafts are Polytetrafluoroethylene or PTFE (Teflon®), Polyethylene Terephthalate or PET (Dacron®), ePTFE (expanded form of Teflon®) and synthetic polymers (e.g. poly-epsilon caprolactone (PCL), polylactic acid (PLA) polyglicolic acid (PGA), polyurethanes (PURs), etc.) [19, 53, ch.128].

The different techniques used to manufacture textile grafts have an effect on the final device properties and on the site for grafting [53]. Woven Dacron® grafts are one of the major choices

available for prosthetic reconstruction in large diameters and are predominantly used in the repair of ruptured abdominal aortic aneurysms, thoracic aorta, and in patients with coagulation defects [19, ch. 128]. These woven structures are formed by interlacing two yarns in a perpendicular fashion. In recent years, the interest in another technique called electrospinning has increased exponentially to create new vascular grafts in small diameters [47]. These fabrics with nano/microscale fibers and a large surface area have a great potential for mimicking the microenvironment of blood vessels. However, their application on humans has not yet been achieved.

Lastly, the research efforts are looking far beyond traditional textile structures and materials to enhance the current grafts. Among the strategies to improve the current vascular grafts are: cellular seeding in the wall (tissue engineering), biodegradable materials for coated prostheses (surface modification), and micro vascular structures [62, 53].

1.2 Problem Statement

It is believed that the success of a textile vascular graft is due to the porous micro-structure of the wall with porosities and pore length scales with an order of magnitude larger than the cell length scale [88, 53]. Some geometric characteristics to define the graft wall are the type of fabric, the degrees of porosity and permeability, thickness, and the specific surface area, among others [45]. For instance, porosity allows different levels of penetration of the cells and the irrigation of fluid with nutrients through the graft wall, providing a scaffold for ingrowth of perivascular tissue in order to obtain a barrier. The permeability prevents bleeding. Both properties are key factors for normal hemostasis after implantation [87]. Hence, the textile wall should be a live prosthesis with the capacity to take part in the tissue repair process. In that biological process, the local fluid dynamics and the cellular transport may be affected by the type of textile vascular graft and the stresses generated by the fluid motion, exerting forces on cells such as pressure effects, drag interaction, and viscous shear stresses, among others [88]. Moreover, it is also believed that the cells around and within the wall react to those forces and convert the mechanical stimulus into biochemical activity through a process known as mechanotransduction [69]. Although the transport of fluids through textiles is of great technical interest in biomedical applications, little is known about predicting the micro-flow pattern into and through the wall. Hence, the first problem that was found with the textile vascular grafts is the difficult task of measuring the local fluid dynamics and the cellular transport *in vivo* and *in vitro* around and inside the wall (i.e., the micro-scale), representing a great deal of research efforts [24]. Many aspects of flow through a fabric can only be understood on a microscopic level [55]. Often, this information is difficult to obtain experimentally. For instance, Laser Doppler Velocimetry or Particle Image Velocimetry (PIV) can only measure the local velocities outer walls, but this is not relevant to quantify the influence of the type of fabric and the shear stress on the cells inside the live graft wall. Additionally, these

experimental techniques need transparent surfaces, but the opacity of the textile surface does not allow this type of measurements [10].

On the other hand, although textile vascular grafts represent a significant advance in patients with cardiovascular diseases, this technology still suffers from several limitations like the formation of clots over its artificial surface [83, 65]. These medical devices have a finite life span which is usually reported based on patency data [19, Ch. 128]. The patency is the ability to remain open and is reported in a percentage. A value of 100% is a totally open lumen. The patency can begin to fall by thrombosis in the early postoperative period of 1 month. When an artificial wall of the graft is first exposed to blood, a process of activation, adhesion and aggregation of platelets will begin, leading to development of thrombus. This clot will narrow the lumen volume acting as an obstacle to the flow and causing a restriction in blood supply to the textile wall, needed for tissue repair, or a distal ischemia on the downstream. Hence, the presence of clots may alter the physiological transport and the local environment of the graft, reducing the flow and may lead to graft occlusion [87]. Occlusion of a graft often results in hospital re-admission and re-operation for the patient. Whereas several studies have concentrated on understanding only the biochemical process of thrombus formation [72, 51], there is a lack of models which are able to show graft occlusion through the transport and deposition of individual platelets over the artificial wall of textile vascular grafts (second problem) [83, 94].

Computational simulations play an important role in the design and evaluation of medical devices, speeding up the initial design before a prototype is developed and reducing experimental tests [21, 29]. Previous computational studies of vascular grafts have focused exclusively on the hemodynamic of end-to-side configurations from a macroscopic viewpoint, changing parameters such as anastomosis angle, graft-to-artery diameter ratio, crimping, and anastomosis shape, among others and considering the blood as a homogeneous fluid [87, 25]. However, the local structure of the textile wall in end-to-end configurations, and properties like permeability and porosity, have not received the attention that they deserve. It is important to quantify the influence of these parameters on the local fluid dynamics at several scales of length and that simultaneously consider the transport and deposition of individual platelets through the artificial wall of a textile graft, related with clot formation, reduction of flow and graft occlusion.

In summary, the phenomena mentioned above involve a wide range of scales and several types of fluid-particle interaction. A computational study would open up the possibilities to explore the multiphysics and multi-scale phenomena around the textile vascular grafts from a biomechanical viewpoint. The goal of this work is to investigate how the type of fabric, permeability and porosity affect both the local fluid dynamics and the fluid-particle interaction among platelets in textile grafts, using a multi-scale approach. Hence, this work expects to answer a key question as: can the behavior of the local fluid dynamics and the fluid-particle interaction among platelets be influenced by the type of fabric, the permeability and the porosity of textile vascular grafts at several scales of length? Thus, this study may be relevant to understand the influence of these design parameters on

mass transport and normal hemostasis after implantation.

1.3 Research Objectives

The main objective of this research is to analyze how the type of fabric, permeability and porosity affect both the local fluid dynamics and the fluid-particle interaction among platelets in textile grafts, using a multi-scale approach.

This problem can be divided into four main research objectives, as follows:

- To formulate a multi-scale mathematical model that represents the behavior of local fluid dynamics and the interaction of platelets in textile grafts in response to changes such as the type of fabric, permeability and porosity.
- To develop a code from the multi-scale mathematical model, using a numerical approach for coupling of a continuum method and a particle method.
- To characterize the permeability and the porosity of several geometric representations of the micro-structure inside the graft wall, using both computational and experimental methods.
- To evaluate the influence of the type of fabric, permeability and porosity both on local fluid dynamics and on fluid-particle interaction among platelets in textile grafts.

1.4 Outline and Scope of the Thesis

The manuscript is organized as follows. The first part presents an introduction of the textiles as vascular grafts, problem formulation, research objectives and scope of the study. The second chapter presents a review of the literature on computational studies related with: vascular grafts, fluid transport through textiles, blood flow on a cellular scale and the development of multi-scale methods for modeling both blood flow at macro-level and cellular response at micro level.

The third chapter is an article that presents a computational and experimental study of the textiles as vascular grafts at several length scales. The aim of the experimental work is to show the micro-structure and to measure permeability and porosity, according to ISO7198 international standard. The aim of the computational work is to quantify the influence of the type of fabric, permeability and porosity both on local fluid dynamics and on fluid-particle interaction among platelets, related with the graft occlusion. The textile wall is considered as a porous media with two scales of length: straight tubular structure with porous walls for the macro-domain and representative unit cells of fabric for the micro-domain. Two types of fabric are considered: woven and electrospun samples. Blood is considered with two phases: suspension of platelets in plasma. The fluid-particle interaction is accomplished in one-way.

The fourth chapter is an article that presents the implementation of a numerical case as one of the main applications of textile vascular grafts to repair Abdominal Aortic Aneurysms (AAA). This chapter includes the computational reconstruction of a infrarenal aneurysm based on a Magnetic Resonance Angiography (MRA) image. Additionally, for this issue, the artificial wall of textile graft is defined with a fictitious domain model and is evaluated with different porosities. The fluid-particle interaction is accomplished in two and four-ways. The numerical process is based on a multi-scale approach, which it is explained both in the third and in the fourth chapter.

Finally, in Chapter 5 it recapitulates major findings and contribution of the thesis, and proposes issues inviting future research.

Chapter 2

LITERATURE REVIEW

This chapter is organized in four sections. They show a review of numerical studies related with vascular grafts, micro-flow in textiles, blood flow on a cellular scale, and multiscale modeling of blood flow with Particle-Based methods.

2.1 Synthetic Grafts and Numerical Studies

Anastomosis is a surgical procedure which joins an artery and a graft in two common configurations: end-to-end and end-to-side [87, 97]. The majority of computational studies of vascular grafts have focused exclusively on the hemodynamic of end-to-side configurations and their relationship with the development of intimal hyperplasia and thrombogenicity of the graft wall [87, 97]. The influence of several geometric factors are analyzed such as anastomosis angle, graft-to-artery diameter ratio, crimping, anastomosis shape and length, etc [25].

For instance, Ben Abdessalem et al. [9, 11] show a numerical study of steady and pulsatile flow in a woven prosthesis of 6 mm diameter and demonstrate that the flow near to the wall is influenced by the morphology of crimping. They solved the Navier-Stokes equations using the Finite Element Method and the results are validated using a Laser Doppler anemometer. Additionally, Ben Abdessalem et al. [10] completed their work with another study related with fluid-structure interaction, allowing prosthesis wall motion to couple with blood flow. The solution is based on the Arbitrary Lagrangian Eulerian (ALE) formulation. That work showed several crimped shapes with different levels of low shear stress due to the displacement of the graft walls. The authors concluded that the low shear stress observed in wall crimping can explain the excessive deposition of platelets, as can be observed in *in vivo* grafts, related with thrombosis and intimal hyperplasia.

The primary means of treating stenosed arteries is to provide an alternative path for blood, or an arterial bypass, in order to avoid obstruction and reach the dependent end organ. Another clinical purpose for using vascular grafts is to provide direct access to the blood stream for a patient with renal failure (i.e. arteriovenous fistulas for hemodialysis). Several studies have focused on that type

of grafts [22, p.325]. For instance, Loth, Fischer and Bassiouny [61] describe the influence of some parameters governing blood flow in end-to-side anastomoses (e.g. the influence of geometry, flow division, and Reynolds number of Newtonian flow in rigid vessels) and the relative importance of their long-term patency on graft failure. The authors focused on two distinct surgical reconstructions, namely, arterial bypass (AB) and arteriovenous (AV) grafts. They show that although both geometries are similar, there are differences in the flow conditions. In AB grafts, there are laminar flows, whereas AV grafts can lead to transitional or weak turbulent flows. Thus, they concluded that intimal hyperplasia (IH) may be different in each case.

Longest et al. [60] conducted a numerical study about platelet-wall interaction at end-to-side anastomoses and their role in the formation of Intimal Hyperplasia (IH). That study was based on parameters such as Wall Shear Stress (WSS) and Near Wall Residence Time (NWRT). NWRT is a nondimensional parameter that indicates the probability of particle deposition [25, p.264]. Sites of significant particle-wall interaction with points of stagnation and elevated concentrations in different geometries, were identified by the model.

Optimization in vascular grafts has been another area of study that has found correlations between hemodynamic and thrombogenicity of the graft wall. Lei et al. [54] and Loth et al. [61] used an iterative optimization procedure coupled with CFD and analyzed the distribution of distal anastomotic wall shear stress, stagnation point flows and separation zones for conventional geometries and optimized geometries. The aim of that work was to obtain a graft configuration designed to reduce separation and stagnation zones.

Another study about shape optimization is presented by Probst et al. [75]. The authors present the sensitivity of optimal shapes of bypass grafts with respect to the non-Newtonian nature of blood, in particular, with respect to kinematic viscosity. Shape optimization framework is coupled to a finite element solver, in order to analyze the shear stress, which has an impact on platelet aggregation. They found that a flattening of the circular shaped bypass reduces the shear stress.

In a further study, Leuprecht et al. [57] show numerical results by means of the finite-element method and analyzed the flow dynamics and wall mechanics at the suture line related to two different surgical techniques: conventional anastomoses and Miller-cuff. The comparison between the two configurations of anastomoses demonstrated less stagnation points in the Miller-cuff, favoring the patency of the graft, as it is found in the *in vivo* Miller-cuff prosthesis.

On the other hand, the majority of studies have focused on planar graft configurations and only few works study non-planarity in graft configurations. For instance, Papaharilaou et al. [68] presented a computational study under both steady and pulsatile flow conditions with two geometric configurations for end-to-side anastomoses: one where the centrelines of bypass and host vessels lie in the same plane, and one where they lie out of the plane of symmetry. The authors concluded that the non-planar model reduces stagnation flow (low shear) regions, promoting the fluid mixture and could favor an improved hemodynamic environment in the anastomosis.

Giordana et al. [42] studied the effects of graft angle (26, 30, and 80 degrees) in distal anas-

tomoses of Arterial Bypass (AB) grafts, analyzing the distribution of wall shear stress and the transport of fluid particles. The models which were studied, with Reynolds numbers in the range of Re = 135–340, indicated different degrees of fluid mixture with the variation of graft angle. They concluded that for shallow angles, slower particles moved to the wall into the proximal outflow segment (POS), predisposing the graft wall to an early occlusion.

Garcia et al. [41] showed a computational study about flow variables such as shear stress, secondary flows and residence time, involved in platelet activation and thrombogenicity of a vascular graft. Computational simulations were developed in Ansys® and Matlab®. Several geometries were built based on the injection-corrosion technique and angiographic images, varying the relation of the diameters of both the anastomosis and the graft. The results presented an acceleration in the anastomosis and secondary flows with low rotational speed after the anastomosis, when the relation of diameter was large. Consequently, activated platelets could fall into these zones and promote aggregation of platelets, resulting in sudden graft occlusion.

The majority of computational studies of vascular grafts have focused exclusively on the flow pattern without considering the presence of the textile graft, changing several geometric characteristics in anastomoses of bypass grafts and relating hemodynamic conditions to the graft failure. Additionally, the blood is considered as a homogeneous fluid in those studies from a macroscopic viewpoint.

2.2 Micro-flow in Textiles and Numerical Studies

The transport of fluids through textiles is relevant for many applications such as parachutes, airbags, geotextiles, filters, sport and protective clothing, biomedical textiles and processes such as the liquid composite moulding process, dyeing and drying of fabrics, to name just a few [55]. So far, most computational studies have focussed on simulations of flow through a textile and have predicted the permeability, as part of the manufacturing process of composite materials [66, 92], but few have researched on textile vascular grafts.

Leisen and Farber [55] presented a combination of two techniques for the study of micro-flow in textiles: Computational Fluid Dynamics (CFD) and Magnetic Resonance Imaging (MRI). The latter technique provided a non-destructive way to predict flow rates within a textile. The modeling of the sample fabric was made with the Nuclear Magnetic Resonance Imaging technique (NMR), optical micrographs and the software MIMICS, allowing the visualization of flow and size of porous structures.

Ngo and Tamma [66] showed permeability predictions for complex geometries of textiles, related with composite molding processes. The authors showed a three-dimensional unit cell of a woven fabric and apply the Finite Element method to predict effective permeabilities. Due to low Reynolds, the Stokes equation was used to model the flow in the inter-tow region (i.e., free flow) and

Brinkman's equation was used in the intra-tow region (i.e., yarn is treated as permeable). Quadratic and hexagonal arrangements of fiber filaments are employed as the intra-tow region. Values of pressure gradients ranging from 1 to 10 Pa/cm and viscosity values between 0.01-1.0 Pa s were also used. The permeability obtained from those different pressure and viscosity combinations, differ by no more than 3%; therefore, the authors concluded that permeability should only be a function of the geometry of the fabric.

Verleye et al. [91] presented another work related to the impregnation stage of a composite material. That numerical study presents a mathematical model to predict the permeability for several types of reinforcements such as plain woven fabric, non-crimp fabric, mono-filament fabric and a random mat. A finite difference Stokes solver and PETSc library were used to solve the problem. For the creation of the textile models, the authors used Wisetex and Flowtex software [52]. The findings showed that textiles with a high volume fraction, intra-yarn flow have a significant influence on permeability value.

Nabovati et al. [63, 64] showed a work to calculate permeability as a function of porosity using the Darcy's Law model and Lattice Boltzmann Method (LBM). Small pressure gradients drove flow and the results were compared with analytical models at several porosities. The authors predicted the effective permeability, considering two different length scales: yarn porosity and weave porosity. The findings of that study indicated that higher weave and yarn porosities result in higher permeability values of the woven sample. Additionally, at lower weave porosities, yarn porosity effect becomes important.

Another work related to textile composites was presented by Belov et al. [15]. The prediction of the permeability was obtained using the Lattice Boltzman Method (LBM), varying the dimensions of tow cross-section and the level of deformability. The threads of yarn were placed with different spacing in weft and warp direction (i.e., different fabric volume fraction) in the unit cell. Additionally, the authors included different values of thickness, varying the number of layers and the level of compression of the unit cell. The findings indicated that the permeability is higher when pore size is higher.

The findings from this section indicate that the geometry, the position and size of the free space in a fabric affect its permeability. The type of textile graft and its local structure may be relevant in the transport phenomena and cell mobility through the interstices of the graft wall from microscopic viewpoint. Moreover, the development of new textile grafts may be improved if details of the flow pattern through the graft wall are known and predicted, before the graft is manufactured.

2.3 Blood Flow on a Cellular Scale and Numerical Studies

Several computational studies, treating blood as a suspension of cells in plasma, have also been reported in literature in order to understand the behavior of blood cells in various flow regimes,

including the deformable nature of red blood cells and cellular response of platelets under pathological conditions [83, 94]. In several of those studies, platelets were considered as point rigid particles that are suspended in Newtonian fluid and transported by convection and shear-enhanced diffusion. For instance, Almomani et al. [12] studied platelet-Red Blood Cells (RBC) interaction as a function of the hematocrit and the Reynolds flow number in shear flows at micro-scale dynamics using the Level-Set Sharp-Interface Immersed Boundary Method. The authors found that the formation of mural thrombi is influenced by platelet-RBC interaction and with high hematocrit values, the platelets move toward the walls while RBCs move to the core region of the vessel.

Leopold et al.[46] presented a multi-scale simulation in a patient with a brain aneurysm, focusing on the interaction of blood cells with the arterial walls that leads to thrombus formation and aneurysm rupture. That study coupled continuum simulations solved by Nektar [7] (a multi-level parallel spectral element solver) with a Molecular Dynamic solver based on Dissipative Particle Dynamics (using Sandia Code LAMMPS [77]). Blood flow through the brain is a multiscale problem and the authors considered both micro and macro scale solutions, key factor for realistic physical and biological systems.

Ken-ichi et al. [85] proposed the moving particle semi-implicit (MPS) method using the Earth simulator (ES) system [82] to analyze the microscopic behavior of blood flow applied to two cases: the motion and deformation of a single RBC, and the thrombogenesis caused by platelet aggregation. In the first case, a RBC membrane was modeled with a small number of particles in a micro-channel, showing changes in its shape, a concave shape on the upstream and a convex shape on the downstream. Additionally, the authors analyzed a primary thrombogenesis caused by platelet aggregation to an injured vascular wall, changing the blood flow velocity. In the region near the injured wall within a specific distance, the probability of aggregation of the platelets was assumed to be higher. This probability was expressed by introducing an attractive force acting between the aggregating platelets and the injured wall, behaving as a solid material. Similar results were obtained by Pivkin et al. [72, 71].

On the other hand, several studies have focused on detailed and accurate models for describing blood-plasma separation problems in channels and bifurcating microfluidic tubes [58]. This procedure is important in medical laboratories which require the separation of RBCs from the whole blood. For instance, Xuejin Li et al. [58] used a model with a wide range of hematocrit levels based on the Dissipative Particle Dynamic method to study the motion of a suspension of red blood cells (RBCs) flowing in a Y-shaped bifurcating microfluidic channel at low Reynolds. The simulations for healthy and malaria-infected blood were performed using the atomistic code named LAMMPS [77] and a modified velocity-Verlet algorithm. The findings from that study showed that separation efficiencies of malaria-infected blood are lower than healthy blood and that low hematocrit levels increase the separation efficiency.

Sandor I. Bernad et al. [78] reported a 3D model of serial stenoses based on tomography images and studied the effects on hemodynamic characteristics such as flow separation, wall shear stress

and particle deposition. The authors found that the multiple stenoses produce more resistance to flow than a single stenosis of similar length. GAMBIT® and ANSYS-FLUENT® were used to solve the computational problem. Carreau Yasuda model was used for the blood. Some particles were deposited on the wall, and others were convected downstream. The authors concluded that regions, with a high particle deposition, correlates well with low WSS contour areas.

Frequent thrombosis and occlusion still constitute a drawback in the use of cardiovascular devices like vascular grafts [79]. The findings from previous studies include the thrombus formation in blood vessels under pathological conditions, but not consider the blood-material interaction with the porous wall of a textile graft, including the activation, adhesion, and aggregation of platelets. This cellular response of individual platelets on artificial surfaces may block the wall, altering the normal circulation.

2.4 Multi-scale Methods for Modeling of Blood Flow with Particle-Based Methods

There are several challenges when attempting to model the behavior of the blood flow from a biomechanical viewpoint [94]. The blood is not merely a continuum fluid, but that it is composed of various cellular components. An approach based purely on a continuum assumption may fail to model biological process related to blood cell-material interaction and thrombus formation in cardiovascular devices. Although various numerical methods have been proposed for blood flow analysis [51], such as the Boundary Element method, the Lattice Boltzmann method, the Immersed Boundary method, there is growing interest in the particle-based Lagrangian methods. This section attempts to describe a few of them.

There are several discrete particle methods used in the numerical simulations of bioengineering problems such as the Molecular Dynamics(MD), the Discrete Element Method (DEM), the Stokesian Dynamics Method (SDM), the Dissipative Particle Dynamics (DPD), the Smooth Particle Hydrodynamics Method (SPH) [59], the Moving Particle Semi-Implicit Method (MPS), among others[94, 51]. For instance, MD and DEM have demonstrated to be efficient to calculate multiple body interaction in a suspension. MD has been used to calculate the hydrodynamic forces and DEM to include biochemical processes during the thrombus formation [94]. Moreover, DEM is similar to MD, but the first one is generally distinguished for considering rotational degrees-of-freedom. In the same way, MPS method has been used for modeling deformable Red Blood Cells (RBCs) and does not require a computational mesh, so simulations can be stable even for problems involving many cell-cell interaction.

During the last decade, another direction that has been taken is the development of multi-scale methods, which couple continuum methods and discrete particle methods [76, 30]. One of them is the Mesoscopic Bridging Scale (MBS) method, which couples the FE method and the Dissipative

Particle Dynamics (DPD) method through force terms [81]. For instance, Kojic [50] presented a methodology of coupling based on MBS for fluid flow. Two case studies were presented in that work: unsteady flow between two plates and fluid flow in a micro-channel with narrowing. Another approach is a DEM-FEM model presented by Rojek and Oñate [76] for dynamic problems with fracture propagation. The authors have implemented additional kinematic constraints imposed by means of penalty functions and Lagrange multipliers. Additionally, the Particle Finite Element method (PFEM) is another approach which eliminates the convective terms in the continuous fluid mechanics equations and uses the Alpha Shape Method for boundary recognition [67, 8].

These coupling methods would be particularly attractive for modeling blood flow and cellular response in textile vascular grafts, providing an insight both on local hemodynamics at macro level and on interaction between blood constituents at a micro level. Thus, the Finite Element Method (FEM) is a traditional method that employs macroscopic models based on the continuum theory to analyze blood flow as homogeneous fluid [50]. Particle based methods are developed to solve physical problems with solid blood cells, where the continuum-based methods are insufficient. Combining both methods in one model will allow one to take advantage of each method for simulating blood flow on a blood cellular scale.

In summary, the review of this chapter highlights that to date, the majority of computational studies of vascular grafts have focused exclusively on the flow pattern at a macro level without considering the presence of a textile vascular graft. The type of fabric, its permeability and its porosity to define the textile wall in anastomoses of end-to-end configurations have not been considered in order to evaluate the influence on local fluid dynamics at several scales of length. Also, in general, the blood is commonly treated as a homogeneous fluid. Blood is not merely a monophasic fluid, but it is composed of various cellular components such as platelets, related with the clot formation, reduction of flow and graft occlusion. An approach based purely on a continuum assumption may fail to capture the interactions of those cellular components. There is a need for research these effects better by adopting multi-scale models that include the textile wall as a porous media, the plasma flow as well as the motion of individual platelets in textile vascular grafts.

Chapter 3

BLOOD FLOW AND CELLULAR INTERACTION THROUGH DIFFERENT TYPES OF TEXTILE VASCULAR GRAFTS

3.1 Introduction

Nowadays, innovative applications and research in medical textiles are developing at an important rate, with achievements in several fields as implantable devices, regenerative medicine, bandaging and pressure garments, wound healing, controlled medication release, among others [14]. One of the main advantages of medical textiles are their flexibility, their mechanical properties as well as the wide variety of textile structures such as woven, knitted, non-woven, composite materials, nanofibres, etc. For instance, woven grafts are used predominantly in the repair of the ruptured abdominal aortic aneurysms. On the other hand, nanofibres created using electrospinning are very attractive for this kind of application due to their unique properties such as porosity, micro-scale fibre diameter and high surface area in small vessels [19]. Moreover, modern techniques such as nanoapplications and tissue engineering are beginning to have a great impact on the new textile vascular grafts.

Porosity and permeability have been identified as two key properties to control the flow and nutrients through the wall and simultaneously promote tissue repair in textile vascular grafts after implantation [45]. The permeability of a fabric is the ability to permit the transport of fluid through narrow pores of the wall and the porosity is defined by the ratio of free space to fiber in a given volume of fabric on which the cells can migrate, adhere, proliferate, and differentiate [87, 88, p.53]. These properties can be adjusted in a wide range and are affected by factors such as type of fabric, thickness, yarn size, yarn spacings, among others. The performance of a textile vascular

graft is determined by several functional requirements such as: fluid control, physical barrier, rapid healing, bleeding control, different levels of penetration of the cells, among others, yet predicting the flow rate and cellular transport are still not widely understood and many questions remain open [24, 14].

The aim of this chapter is to investigate how the type of fabric, and its permeability and porosity affect both the local fluid dynamics and the fluid-particle interaction of individual platelets in two types of textile grafts, using a multi-scale approach.

The local structure of the textile wall in end-to-end configurations, and properties like permeability and porosity, have not received the attention that they deserve. This chapter provides insight into the importance of these parameters on the titanic task of trying to improve the design of textile vascular grafts.

3.2 Methods

This section describes both computational and experimental tests of textile vascular grafts. The aim of the experimental work is to show the micro-structure and to measure permeability and porosity, according to ISO7198 international standard [3]. The aim of the computational work is to quantify the influence of the type of fabric, permeability and porosity both on local fluid dynamics and on fluid-particle interaction among platelets, related with the graft occlusion.

3.2.1 Textile Modelling

One of the major challenges for modelling of an accurate and appropriate virtual textile model is the structure topology [33, 66]. The specific geometry can be obtained from mathematical models (for simple cases) or experimental tools like microscopic techniques. For instance, a technique to acquire images for the micro-structure of a textile is Scanning Electron Microscope (SEM). This technique allows to visualize the internal structure and surface characteristics in opaque substrates like the textiles.

Two types of samples were analyzed in this work with SEM technique: woven and electrospun. Commercial grafts were used like woven samples and the electrospun samples were manufactured from Poly-Urethane (PU) polymers, using the electrospinning technique, Fig. 3.2.1.

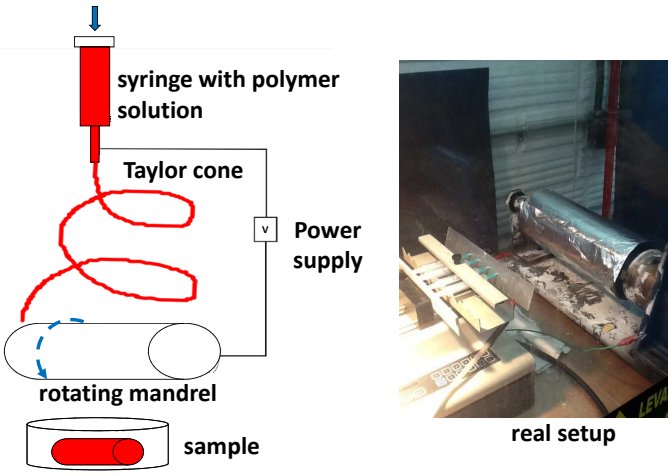

Figure 3.2.1: Electrospinning setup: schematic representation of a electrospinning machine (left) and pictures of the real setup (right).

Electrospinning is a common technique used to fabricate micro-nanofibres [16]. Several manufacturing parameters must be considered such as: number of needles, needle size, voltage, speed of collector, needle-collector distance, and flow rate, among others [47]. By varying the parameters, samples with different porosities, pore size and fiber diameter can be obtained. The principle of fabrication is simple: the synthetic polymer is prepared with a solvent at a certain temperature. Later, the solution is charged into a syringe and is pumped at a slow flow rate. A DC voltage is applied to the solution. As the solution travels from the syringe toward the collector, the solvent evaporates and makes a cone shape called the Taylor cone. The collector is wrapped with a sheet of aluminum and sprayed with a mold release agent.

Once the samples were obtained and manufactured, micrographs from SEM were analyzed in order to obtain a geometric description of the micro-structure inside the textile wall for virtual models. This test was accomplished with a scanning electron microscope (Phenom). The fabric type, thickness, number of layers, volume fraction, yarn dimensions and spacing in between the yarns, among others properties were measured in order to develop an accurate and appropriate virtual textile model.

Lastly, due to the multi-scale porous structures of textiles, they can be analyzed as a continuum material on the macro-level or as representative unit cells (RUCs) on the micro-level [33]. Ideally, textile has a periodic pattern and the study of a RUC of the layer reveals all relevant information of the fabric. Two scales of length of the textile wall were considered in this work: straight tubular structure with porous walls for macro-domain and representative unit cells for the micro-domain. For the creation of the virtual textile structures for the micro-domain, there are several commercial software such as TechText CAD® [5], WeaveEngineer® [6], ScotWeave® [4], Wisetex® [52], among others. In this work, Fabric Mechanics® software was used for the creation of a unit cell of

woven sample [90, 93] and Rhino® with Grasshopper® software for modeling of an electrospun sample. Once textile models are made, the models are meshed and can be used as direct input for the flow solver.

3.2.2 Permeability and Porosity

As was mentioned before, porosity and permeability have been identified as two key properties in the healing process after implantation [45]. Permeability is a geometric characteristic related to the structural features of a textile at several scales of length [92]. There are several methods to predict permeability, such as analytical formulas (for simple structures), pore network models, numerical models such as FE/FV/Lattice Boltzmann methods via Darcy's law, experimental tests, among others [91]. On the other hand, porosity is a dimensionless parameter defined as follows[27]:

$$\varepsilon = \frac{\text{void volume}}{\text{total material volume}} \tag{3.2.1}$$

In 1962, DuPont® found that this property plays an important role in tissue repair [62, 23]. Porosity can be isolated or connected. It is isolated when the porous spaces are not connected and it is connected when a fluid can flow through the porous spaces [73].

The permeability (k) and porosity (ε) define the transport of fluid and particles within the textile wall [45]. Several variations in fluid velocities are associated with the mechanical dispersion [28]. For instance, differences in the pore size cause the fluid and particles to move slowly or fastly along the graft wall; in path length, the tortuosity causes some particles to move through long or short paths; and lastly, the friction within an individual pore makes the fluid and particles flow at smaller velocities at the pore walls and at higher velocities at the center of the pore, Fig. 3.2.2.

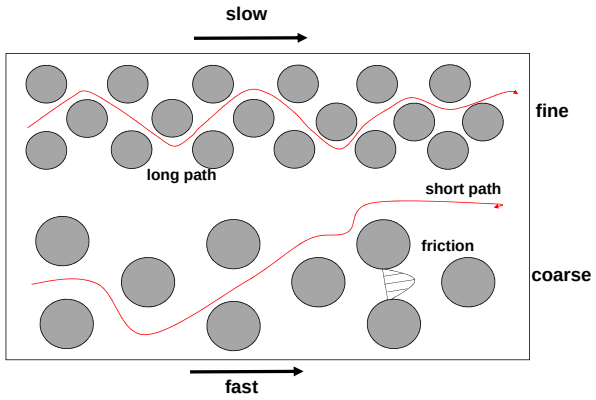

Figure 3.2.2: Particle mass transport due to mechanical dispersion: representation of three phenomena associated to mechanical dispersion (left) and particles interaction inside the wall (right) [28].

3.2.2.1 Experimental Determination of the Permeability and Porosity

The ISO 7198 standard provides basic protocols for permeability and porosity tests of vascular grafts [3, 36, 32]. The porosity test determines the area of the voids of the material on the sample prosthesis. Two methods are used: gravimetric porosity and microscopic porosity. The gravimetric method measures mass per unit area of the sample based on density and wall thickness of the sample:

$$\text{Porosity} = 100 \times \left(1 - \frac{mass}{area \times thickness \times density}\right) \tag{3.2.2}$$

The microscopic method shows the micro-structure and measures the mean of pore size, diameter of the filaments, filament spacing, etc. based on Scanning Electron Microscope (SEM). An analytical balance (model AX200, Shimadzu) and a Scanning Electron Microscope (Phenom) were used for these tasks. Additionally, the wall thickness was measured with a digital micrometer (Mitutoyo).

On the other hand, the water permeability test measures the hydraulic conductivity [(mL/min)/cm^2], which is a measure of water through a given area of the sample under a given hydrostatic pressure. Hydraulic conductivity is computed from the equation:

$$\text{Hydraulic conductivity} = \frac{flow\,rate}{area} \tag{3.2.3}$$

For this test, a vertical column of water is used with hydrostatic pressure values in the range of 80-150 mmHg, Fig 3.2.3. The area of the sample must be between 0.5 cm^2 and 1.0 cm^2, according to the international standard. Distilled water is used to avoid blocking of the pores. The international standard recommends that leaks around the sample are not observed. Then, given the value of hydraulic conductivity, permeability can be calculated as follows:

$$k = K\frac{\mu}{\rho g} \tag{3.2.4}$$

where k is permeability [m^2], K is hydraulic conductivity [m/s], μ is the dynamic viscosity of the fluid [kg/(m·s)], ρ is the density of the fluid [kg/m^3], and g is the gravity [m/s^2].

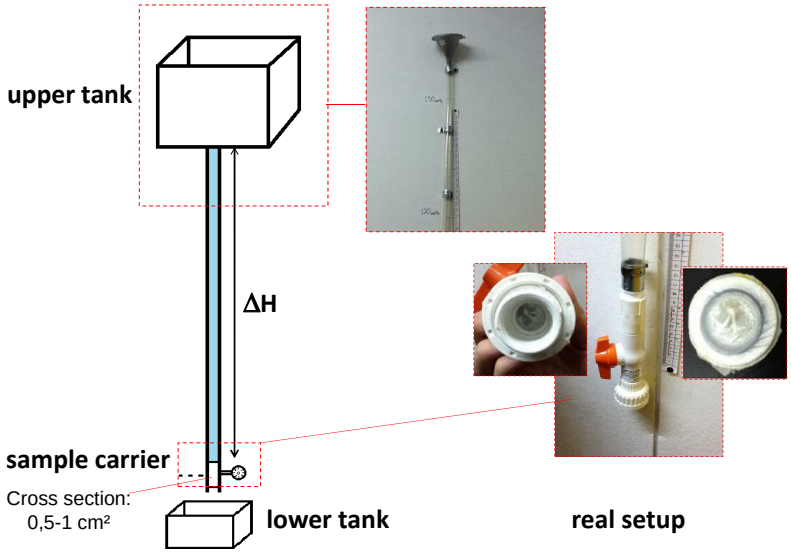

Figure 3.2.3: Permeability setup: schematic representation of a vertical column of water (left) and pictures of the real setup (right).

3.2.2.2 Computational Determination of the Permeability and Porosity

In order to compute the permeability via computational methods, the representative volume elements (RVE) or unit cells of the micro-structure of textile grafts were used, taking advantage of the periodicity of the textile geometry. The Stokes equation is iteratively solved by FEM in those micro-domains and once convergence is reached, using the pressure and velocity fields, the permeability is computed through back substitution of Darcy's law [66]:

$$< \mathbf{u} >= -\frac{1}{\mu}\mathbf{k} < \nabla p > \tag{3.2.5}$$

with $< \cdot >$ is the average value. A summary of the process is presented in Fig. 3.2.4.

The micro-scale permeability and porosity are input for flow simulations on the macro-scale. The variation on the micro-scale has an important influence on the macro-scale. It is important that these variations be captured in a sufficiently accurate way, in order to be able to perform reliable macro-scale simulations.

3.3 Governing Equations

3.3.1 Model Considerations

Due to the complex interaction of all the physical and chemical processes taking place between the blood and the textile vascular graft, it is necessary to consider some simplifications and assumptions

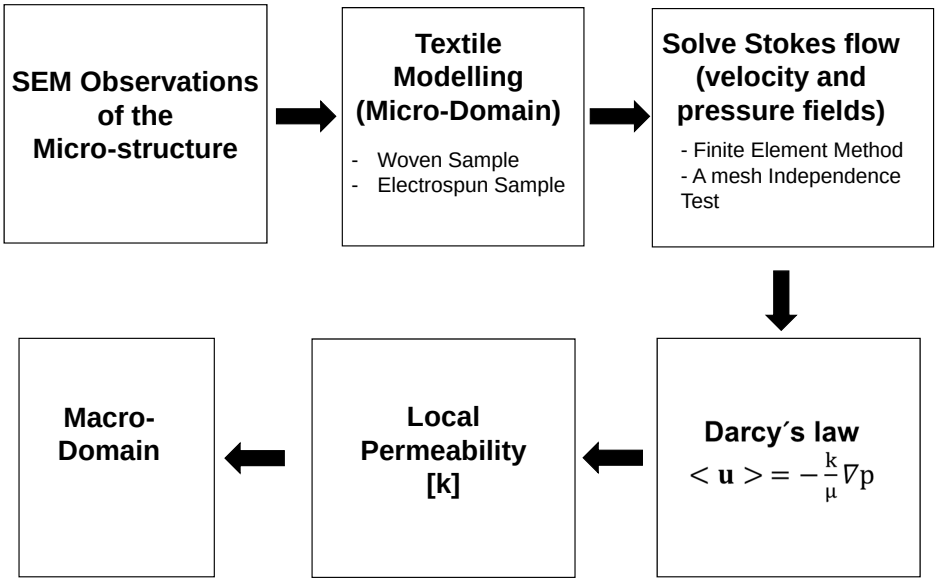

Figure 3.2.4: Flowchart to compute the permeability via computational methods.

in order to computationally solve the problem. The model simplifications and assumptions are as follows:

- The textile wall is considered as a porous media with two scales of length: straight tubular structure with porous walls for the macro-domain and representative unit cells of fabric for the micro-domain.
- The effect of the wall motion is considered neglected. Synthetic grafts are generally stiffer than the native vessels [87].
- The blood is considered as a suspension of platelets in plasma, related with the graft occlusion. Blood plasma is an aqueous solution that can be assumed Newtonian, homogeneous and incompressible with real blood properties: ρ=1.056g/cm^3, μ=3.5cPoise and ν=0.035cm^2/s [25, 9] (see Appendix C).
- The platelets are considered as micro-particles due to their small size. The platelets are the smallest of blood cells, 2 to 3 microns in size [46, 25].
- Chemical interaction and the influence of the electric charge of the cells are not considered.
- Magnus effect is considered negligible, so that there are no particle rotational effects.
- The porous domains are saturated by the moving fluid, so that there are no capillarity effects.

For the purpose of modelling the behavior between a textile vascular graft and the blood at several length scales, treating blood as a suspension of cells in plasma and taking clotting effects into account, different mathematical models are required for each scale.

3.3.2 Blood Flow for Micro-Scale

As was mentioned before, representative unit cells of the textile wall were considered for the description of internal structure for micro-domains, due to the periodicity of the textile geometry. Two configurations were included: woven and electrospun samples, Fig. 3.3.1.

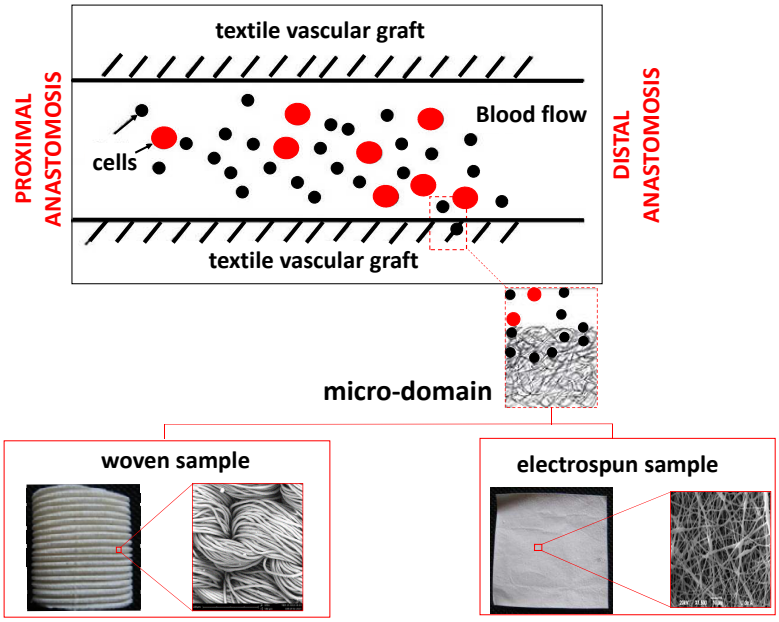

Figure 3.3.1: Textile graft at micro-scale. Unit cell with two possible configurations: woven and electrospun.

At the micro-scale level, the wall of a textile vascular graft offers a local micro-structure with an interconnected pore network, favoring a well-controlled environment for the neovascularization, nutrient supply, and cellular transport [17, p.4]. Usually in a micro-fluidics system, the flow of the carrier fluid is assumed to be steady and with low Reynolds. Hence, the system would be modeled by the steady Stokes equations:

$$\nabla \cdot \vec{u} = 0 \tag{3.3.1}$$

$$0 = -\nabla p + \mu \triangle \vec{u} + \vec{F} \tag{3.3.2}$$

3.3.3 Blood Flow for Macro-Scale

In this case, it is considered a straight tubular structure as the domain of an anastomoses of end-to-end configuration on a large scale (macro-domain). The domain of Fig. 3.3.2 includes a two-dimensional duct of length L, with porous walls located at y=±r. Fluid is injected into the duct at x=0, having a parabolic velocity profile and with a given distribution of particles. It is prescribed a free stress condition at the outlet.

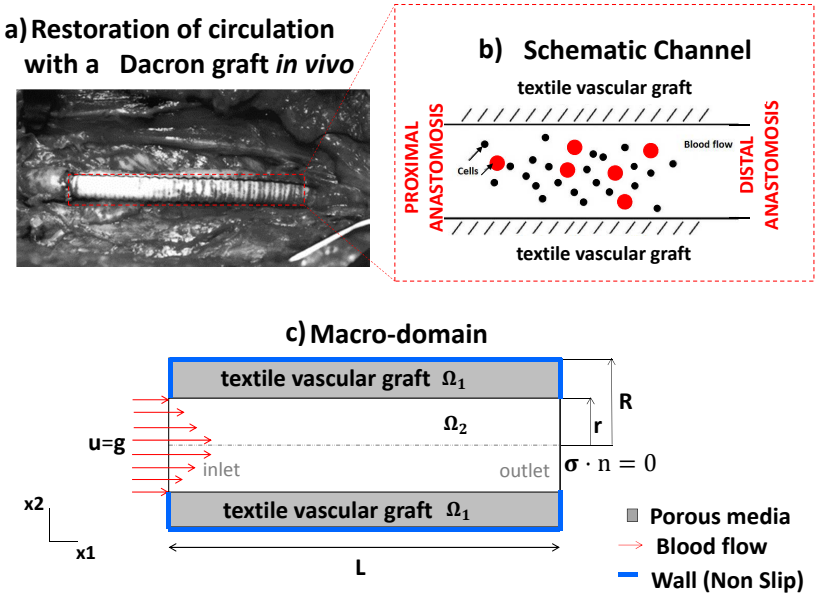

Figure 3.3.2: Textile graft at macro-scale: a) restoration of circulation with a Dacron® graft *in vivo* [39]; b) an idealized duct with porous walls, incorporating an end-to-end configuration and release of cells; c) computational domain.

It is necessary to solve the flow in both the textile and the fluid regions (domain decomposition). The flow in the vascular graft can be modelled as free flow in the internal duct (Ω2) and flow through porous media in the textile (Ω1). The field of free flow is described by the conventional Navier-Stokes equations and the interstitial flow passing through textile graft pores is described by Brinkman's equation [35, 26].

In the free flow:

$$\nabla \cdot \vec{u} = 0 \tag{3.3.3}$$

$$\rho \frac{\partial \vec{u}}{\partial t} + \rho \vec{u} \cdot \nabla \vec{u} = -\nabla p + \mu \triangle \vec{u} + \vec{F} \tag{3.3.4}$$

In the porous media, the system is assumed as a homogeneous medium with a specified porosity and permeability:

$$\nabla \cdot \vec{u} = 0 \tag{3.3.5}$$

$$\frac{\rho}{\varepsilon}\frac{\partial \vec{u}}{\partial t} + \frac{\rho}{\varepsilon}\left[(\vec{u}\cdot\nabla)\frac{\vec{u}}{\varepsilon}\right] = -\nabla p + \frac{\mu}{\varepsilon}\triangle\vec{u} - \frac{\mu}{k}\vec{u} + \vec{F} \tag{3.3.6}$$

where $\vec{u}$ and p are the superficial velocity and the pressure, ρ and μ are the fluid density and fluid dynamic viscosity, ε and k are the porosity and permeability of the porous media, and $\vec{u}/\varepsilon$ is called interstitial velocity, Darcy velocity or filtration velocity. Furthermore, ε and k are defined for the macro-domain based on the results that were obtained by experimental and computational methods from the micro-domain, see section 3.2.2.

3.3.4 Cellular Transport

The kinematics of a cell in the Eulerian-Lagrangian framework may be written as [95, 25, p.100]:

$$m_p\frac{\partial(v_p)}{\partial t} = \vec{F}_{\text{drag}} + \vec{F}_{\text{g}} + \vec{F}_{\text{ext}} \tag{3.3.7}$$

where a particle is defined by its diameter d_p, its mass m_p or density ρ_p and its velocity v_p. In this work, the particles have been defined using the properties of platelets, related with the graft occlusion. The initial position of the particles was selected at the centroid of each element surrounding the nodes in a FEM mesh. This decomposition has a fixed mesh for fluid and rigid particles which can freely move.

The first term of the surface forces is the hydrodynamic drag force, which is calculated as [89]:

$$\vec{F}_{drag} = -m_p\frac{(\vec{u}-\vec{v}_p)}{\tau_p} \tag{3.3.8}$$

where $\vec{u}$ is the velocity of the fluid and the mass of the particle m_p, assuming that the particle is spherical, is defined as:

$$m_p = \frac{1}{6}\rho_p\pi d_p^3 \tag{3.3.9}$$

Particle relaxation time τ_p or momentum response time is the time it takes for a particle to respond to changes in local flow velocity:

$$\tau_p = \frac{4}{3}\frac{\rho_p d_p}{\rho_f C_D \mid \vec{u}-\vec{v}_p \mid} \tag{3.3.10}$$

The friction coefficient C_D for spherical particles is defined as follows:

$$C_D = \begin{cases} \frac{24}{Re_p} & \text{if } Re_p < 1 \text{ Stokes regimen} \\ \frac{24}{Re_p}(1 + \frac{1}{6}Re_p^{2/3}) & \text{if } 1 \leq Re_p \leq 1000 \text{ Transition regimen} \\ 0.44 & \text{if } Re_p > 1000 \text{ Newtonian regimen} \end{cases} \tag{3.3.11}$$

Thus, C_D is a function of the particle Reynolds number:

$$Re_p = \frac{\rho_f d_p \mid \vec{u} - \vec{v}_p \mid}{\mu_f}. \tag{3.3.12}$$

The second term in the equation 3.3.7 represents a combination of the buoyancy and gravitational forces acting on the particle [95, 25, p.100]:

$$\vec{F}_g = \frac{4}{3}(\rho_p - \rho_f)\pi\frac{d_p}{2}\vec{g} \tag{3.3.13}$$

The third term in the equation 3.3.7 represents external forces. These forces may be due to attraction of cells to nutrients in the blood, adhesive forces among platelets and the artificial surface (i.e., textile wall), or aggregating forces between platelets, among others.

3.3.5 One-way coupling

The interaction between fluid and particles occurs in a wide range of engineering problems and applied sciences, which takes the fluid phase as continuous and the particle phase as discrete [67]. The governing equation of the continuous phase is described by Navier-Stokes equations and the particle phase is governed by Newton's second law of motion. This interaction can be in a one-way, i.e. fluid-to-particle forces are transferred to the particles affecting their trajectories but these particles do not affect flow field momentum [89]. Typically, one-way coupling can be used when the discrete phase is diluted, i.e. the volume fraction or the fraction of volume occupied by the discrete phase within a given volume is less than 1% which means that the volume fraction of the discrete phase should be much smaller than the volume fraction of the continuous phase [86], Fig. 3.3.3. For instance, treating blood as a suspension of cells in plasma, the low concentration of platelets in the blood allows for the transport of these cells to be computed in a one-way coupling [25]. That is, a normal range of red blood cells counts for healthy adults is between 4.2 to 6.7 million per microliter of blood, whereas that a normal range of platelets is between 150.000 to 400.000 per microliter.

3.4 Numerical Implementation

A FEM solver in Comsol® was used to solve the flow in laminar conditions and different subdomains both in the porous region and in the fluid region. The interface between Navier-Stokes flow

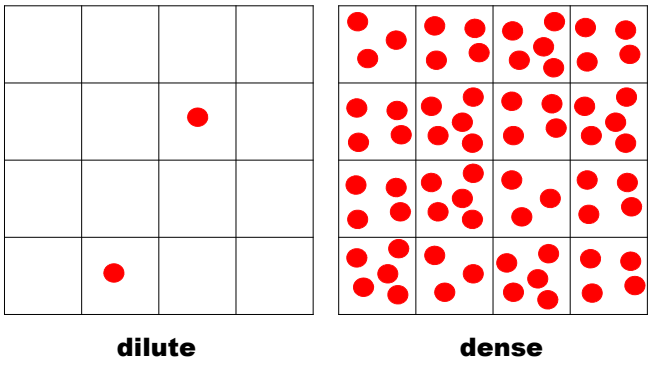

Figure 3.3.3: Dilute and dense flows: dilute flow where less than one particle is present in a computational element; dense flow where a high number of particles are present in a computational element [86].

zone and Brinkman flow zone is coupled with a constraint of continuous velocity, considering that the velocities on both sides of the interface are of the same order [35].

A partitioned approach was used to solve separately the set of equations of flow and particle trajectories with two different solvers. In fact, the Navier-Stokes equations and Brinkman equations were solved together and a steady state solution of flow was first obtained. Then, the set of equations which describe particle trajectories were solved based on the stored velocity field. The particle position was computed using a Lagrangian approach based on a Newtonian formulation by a time dependent solver. The drag and gravity forces were considered.

Moreover, a mesh independence tests were performed for each model both in macro-domain and in micro-domain. Only results from fine meshes are presented. The average mesh quality for all numerical cases of this chapter was superior to 0.92. The Finite Element Discretization method in Comsol® is the Galerkin method in which a weak equation form corresponding to a strong equation is obtained by multiplying with the basis function and integrating over the computational domain. Lastly, the fluid-particle interaction is accomplished in one-way.

3.5 Results and Discussion

3.5.1 Verification and Validation

A first attempt to validate the model was developed in the lab of Dr. M. Nichole Rylander at Virginia Tech in order to validate the model's capability to predict the cell transport under a range of fluid shear stress conditions. Details of the method can be found in [20]. This case was applied

in the oncology field that integrates cancer biology, micro-scale fluid mechanics, and optical flow diagnostics. Briefly, the experimental apparatus includes a 3D microchannel *in vitro* of hydrogel to investigate the cell migration with tumor cells, Fig. 3.5.1 (a and b). Cancer cells were seeded in the wall with endothelial cells seeded along the lumenal surface of the central microchannel, Fig. 3.5.1 (c). Micro-particle image velocimetry (microPIV) was integrated into the system in order to quantify velocity profiles within the microchannel, Fig. 3.5.1(d).

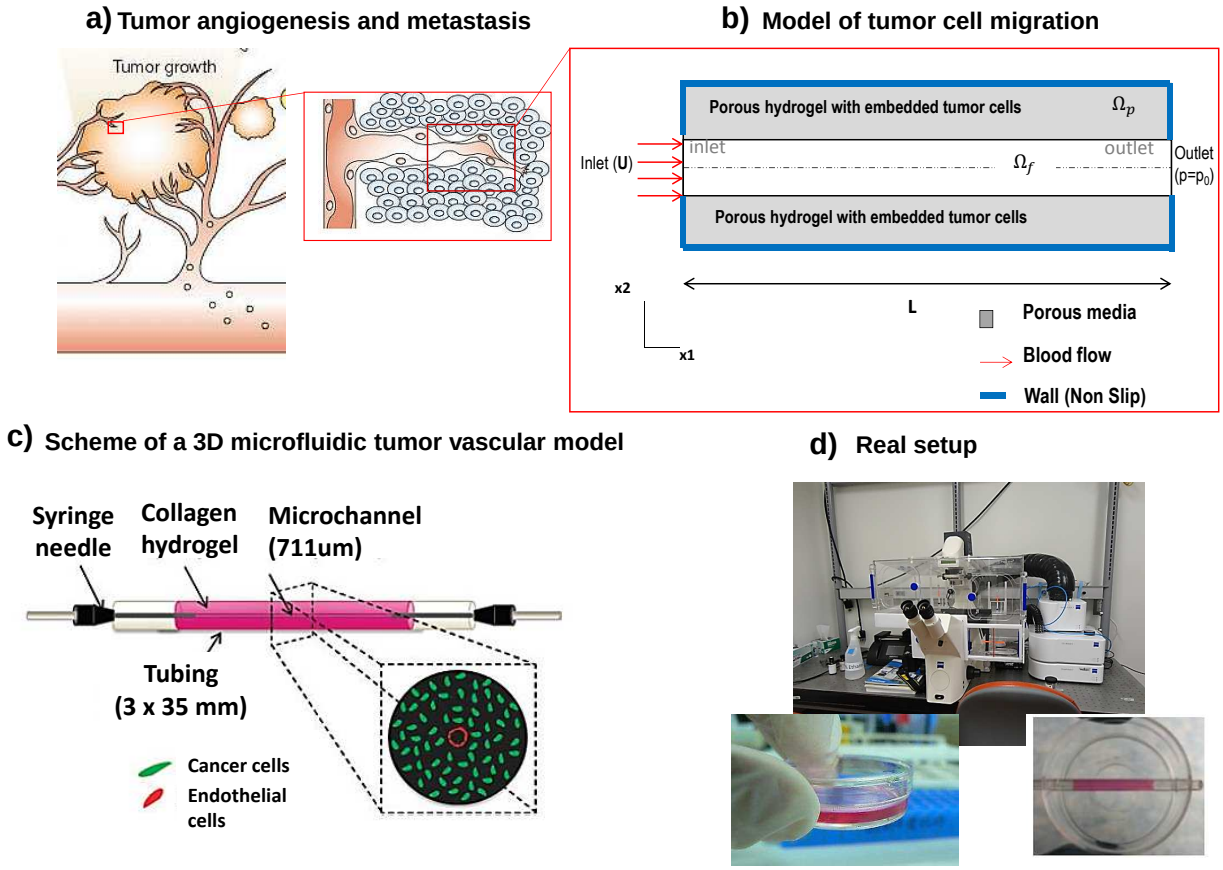

Figure 3.5.1: In vitro breast tumor engineered system: (a) model of tumor cell migration; (b) simplified model of tumor cell migration; (c) scheme for *in vitro* of a 3D microfluidic tumor vascular system; (d) micro-particle image velocimetry (microPIV).

The first step was to create a 3D tumor scaffold, Fig. 3.5.2(a). For this task, type I collagen stock solutions were prepared from rat tail tendons dissolved in a HCl solution. 3D microfluidic hydrogels were fabricated by pouring neutralized solution into a 3 mm fluorinated ethylene propylene (FEP) tubing fit concentrically with a 22G (711 μm) stainless steel needle and stabilized in a standard 35-mm glass-bottom Petri dish. After that, the collagen was polymerized before removing the needle, creating a cylindrical microchannel embedded within the hydrogel. Later, breast cancer cells (MDA-MB-231) were suspended in the collagen during polymerization (1×10^6cells/ml), Fig. 3.5.2(b). To introduce flow, 0.5" 22G needles were partially inserted into the microchannel. Lastly,

the inlet was connected to a syringe pump that controlled the flow rate and the outlet needle led to a collection reservoir, Fig. 3.5.2(c). Additionally, several flow rates were controlled generating a target WSS of 1, 4 and 10 dynes/cm^2. Indeed, average shear stress in a normal microvasculature is 4 dynes/cm^2 [20] and these values were estimated based on an assumption of Poiseuille flow. Then, fluorescent microparticles were injected in the system at defined flow rates and several pictures were taken using a high-speed camera. An image processing technique and automated particle tracking velocimetry (PTV) software were used to calculate the velocity field.

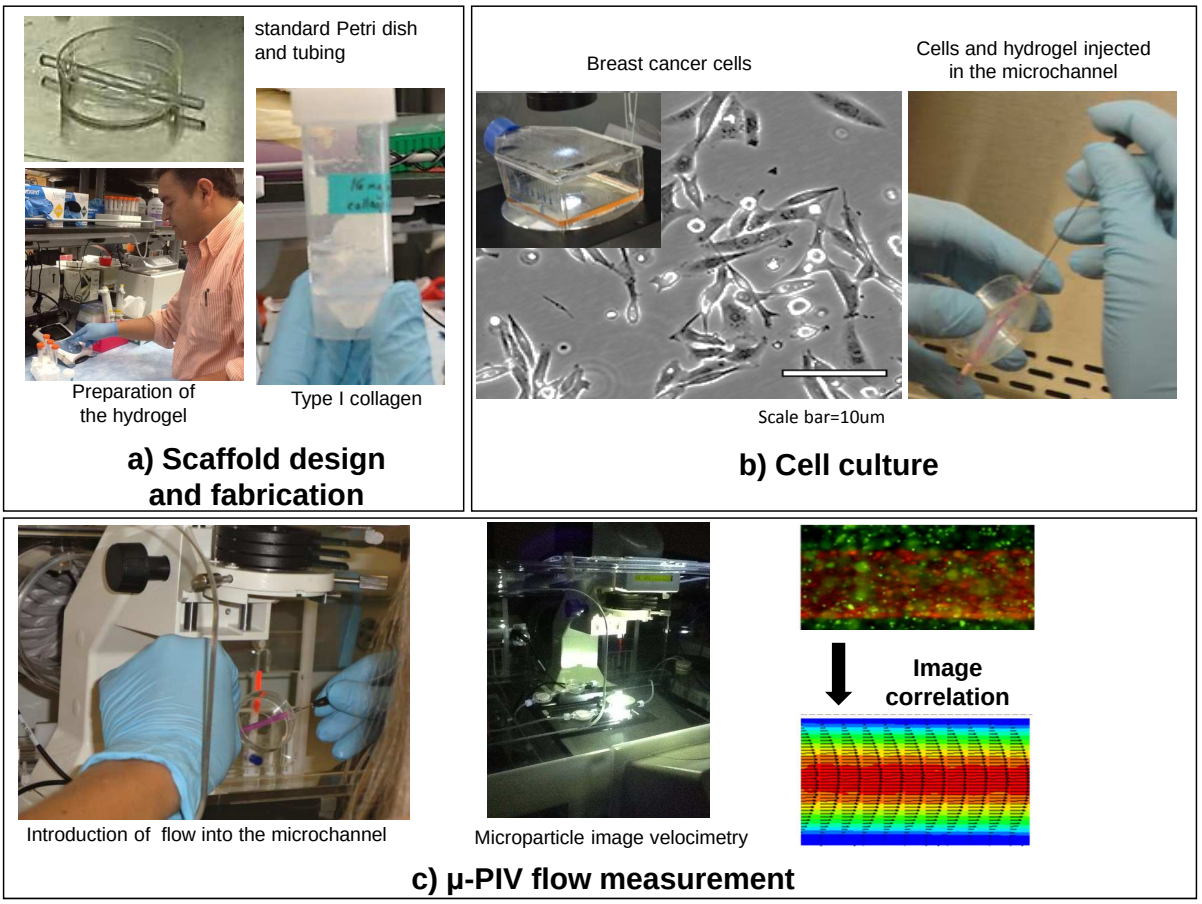

Figure 3.5.2: Fabrication of collagen microchannel and experimental setup: (a) scaffold design and fabrication; (b) cell culture of breast cancer cells (MDA-MB-231); (c) Flow measurement and cell tracking using an image processing technique and an automated particle tracking velocimetry (PTV) software.

Velocity profile was characterized in the collagen microchannel at different flow rates generating a target WSS of 1, 4 and 10 dynes/cm^2. Flow rates were estimated based on an assumption of Poiseuille flow. As a result, velocity data acquired from the experimental data match closely to the numerical solution and to the estimated parabolic Poiseuille solution, in all cases of flow conditions, Fig. 3.5.3. However, slight differences with a relative error less than 8.48% in experimental versus simulation and analytical solutions could be because of resolution limitations in PIV.

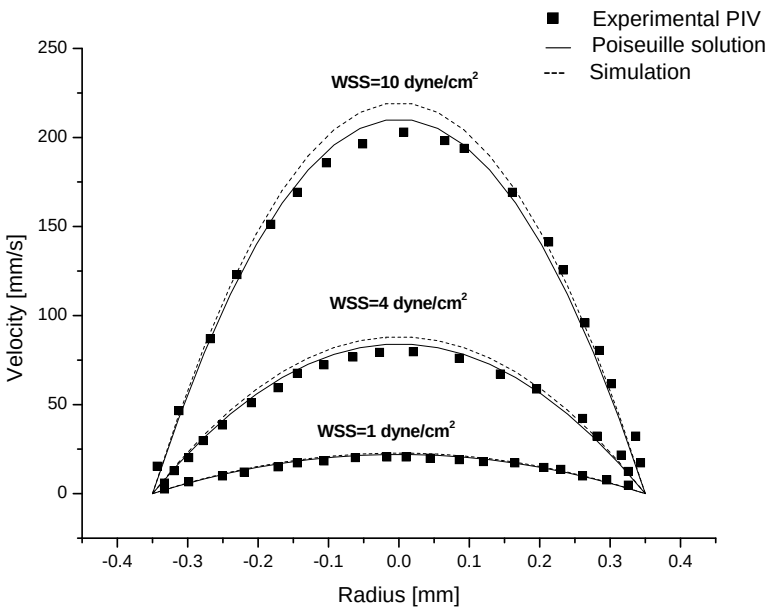

Figure 3.5.3: Experimental, computational and Poiseuille solutions for in vitro breast tumor engineered system. Velocity profiles in mm/s.

3.5.2 Computational Reconstruction of the Textile Samples

As was mentioned before, two types of samples were analyzed: woven and electrospun. The woven prosthesis was a commercial sample of polyester with 8 mm diameter. The electrospun samples were manufactured with thickness values in the range of 82-1000μm. This range was considered based on the thicknesses of commercial grafts and vessel walls. Some parameters of the electrospinning process are listed in Table 3.1:

Once the samples were obtained and manufactured, micrographs from SEM were analyzed in order to obtain a geometric description and variability of the micro-structure inside the textile wall, Fig. 3.5.4. The aim was to extract geometric data such as the mean of pore size, diameter of the filament, filament spacing, etc.

Table 3.1: Parameters of the Electrospinning Process.

Manufacturing Process Parameters	Values
Number of needles	10
Needle size (gauge):	21
Voltage [kV]:	14
Speed [rpm] of mandrel: approx.	36
Needle-mandrel distance [cm]:	14-16
Flow rate [ml/h]:	0.25

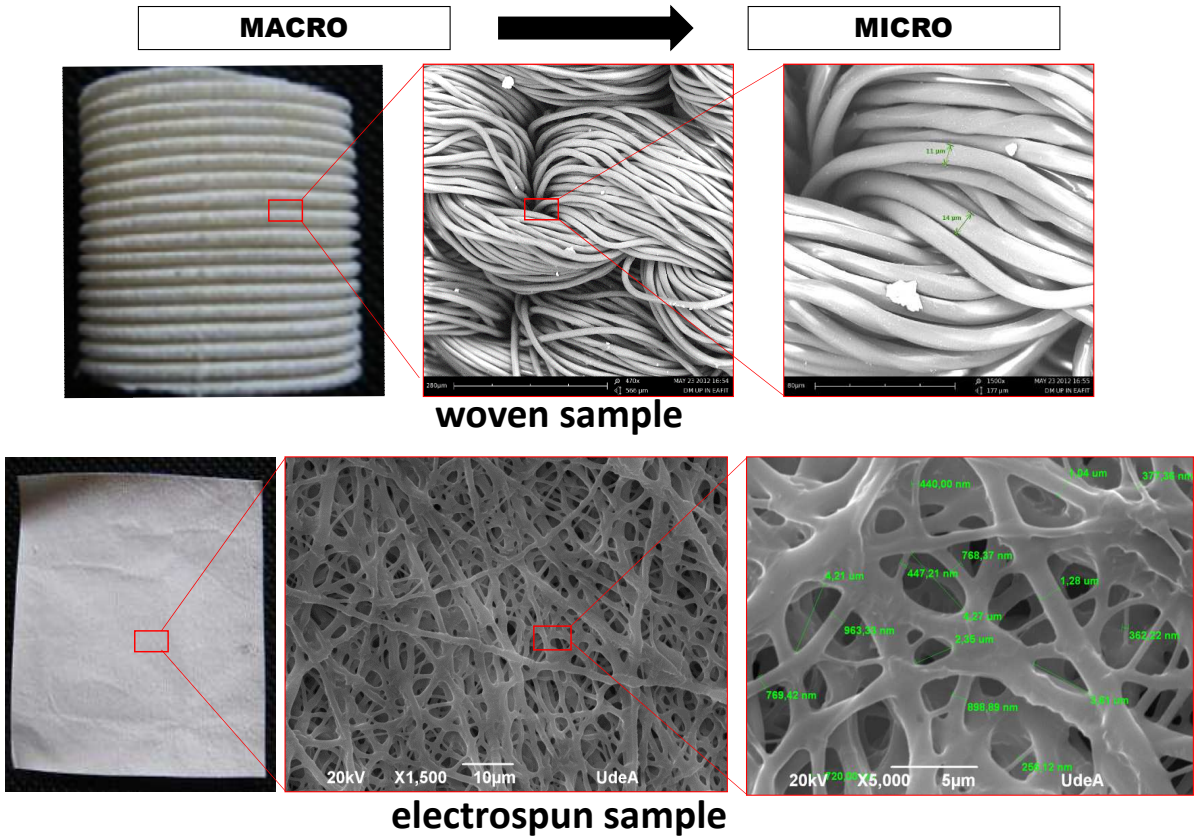

Figure 3.5.4: SEM micrographs of the textile grafts: woven sample (top) and electrospun sample (bottom). Scale bar for woven sample: 280 and 80 μm. Scale bar for electrospun sample: 10 and 5 μm.

Figure 3.5.5 shows 3D geometric representations of the micro-structure of fabric, both for woven and electrospun samples, based on data from SEM micrographs. For instance, to create the woven fabric unit cell, the cell topology was defined by the thickness, number of layers and weft and warp yarn pattern. To create the electrospun unit cell, cylindrical and straight filaments of constant diameter are randomly placed in a cubic domain with free overlapping based on the volume fraction, thickness, diameter and length. These CAD models were used in simulations to predict permeability and blood-material interaction for the micro-domain.

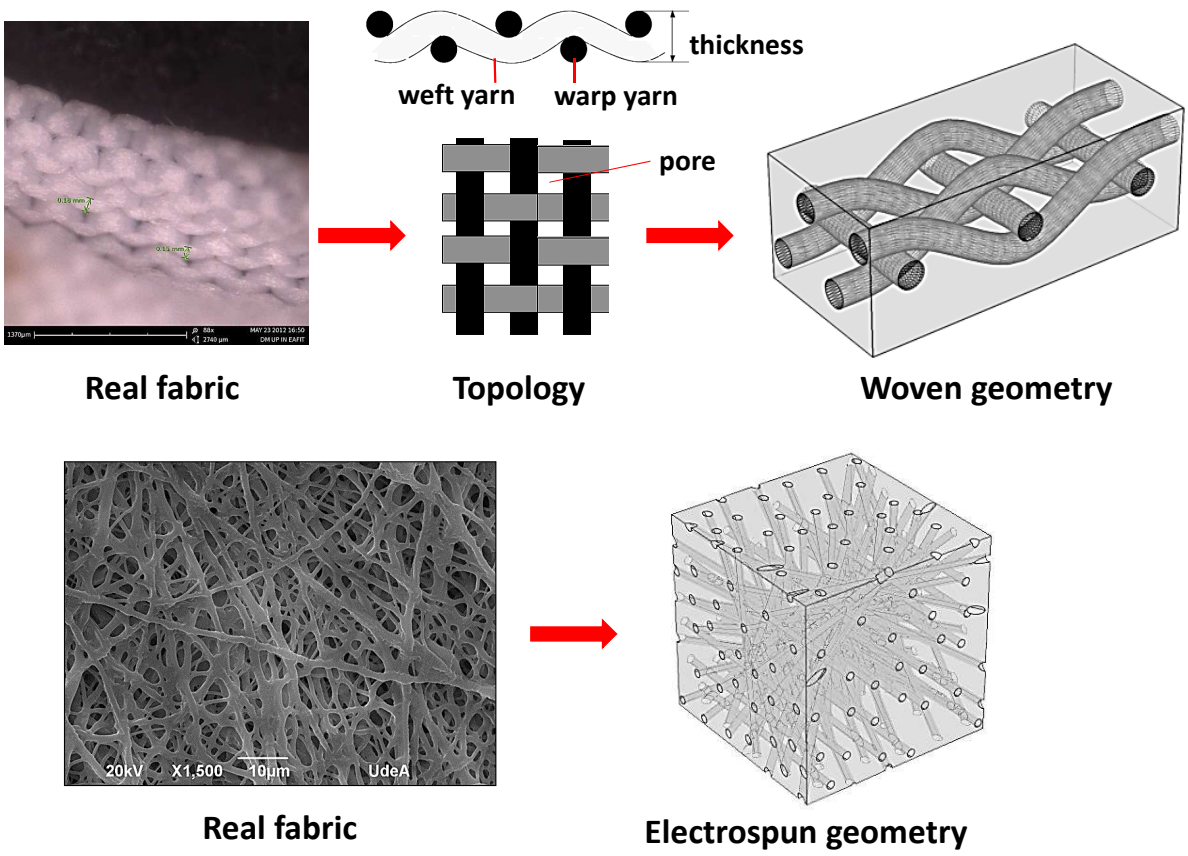

Figure 3.5.5: 3D geometric representations of textile grafts: woven geometry (top) and electrospun geometry (bottom).

3.5.3 Characterization of Permeability and Porosity Both for Woven and Electrospun Samples

The purpose of this section is to evaluate the permeability and porosity both for the real samples and the virtual models. As was mentioned before, woven and electrospun samples were considered. The first part presents the characterization of permeability and porosity by experimental methods, according to the ISO 7198 standard. The last part predicts the permeability and porosity for the representative volume elements (RVE) of virtual models by computational methods. Permeability is computed through back substitution of Darcy's law using the computed pressure and velocity fields.

3.5.3.1 Experimental Method

Hydraulic conductivity $[(\text{mL/min})/\text{cm}^2]$ was first evaluated, which is a measure of water which can flow through a circular sample, with an area of 1 cm^2 under physiological pressure conditions. Figure 3.5.6 shows some hydraulic conductivity values of the woven sample, in the range of

50-300 (mL/min)/cm^2. Thickness and porosity were 0.491 mm and 80.89%. According to literature [87, 45], these results for woven fabrics were within the same range as those studies (i.e. less to 1000 (mL/min)/cm^2).

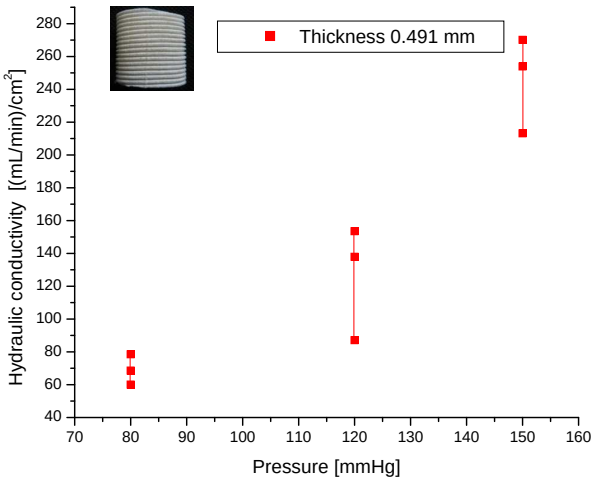

Figure 3.5.6: Experimental hydraulic conductivity [(mL/min)/cm^2] values with hydrostatic pressure values at 80, 120 and 150 mmHg for the woven sample.

For electrospun samples, hydraulic conductivity values were obtained in the range of 4-24 (mL/min)/cm^2, Fig 3.5.7. The thickness and porosity were 0.4950 mm and 63.41% for the sample 1 and 0.9474 mm and 71.99% for the sample 2. Polyurethane samples were within the range of less than 30 (mL/min)/cm^2, corresponding to this type of materials, according to literature [87].

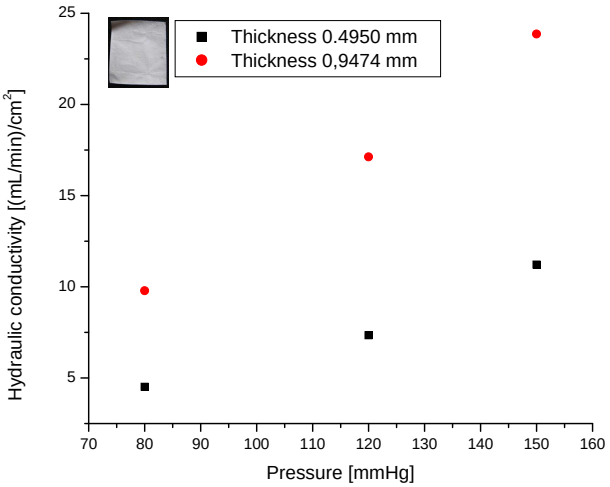

Figure 3.5.7: Average of experimental hydraulic conductivity [(mL/min)/cm^2] values with hydrostatic pressure values at 80, 120 and 150 mmHg for electrospun samples.

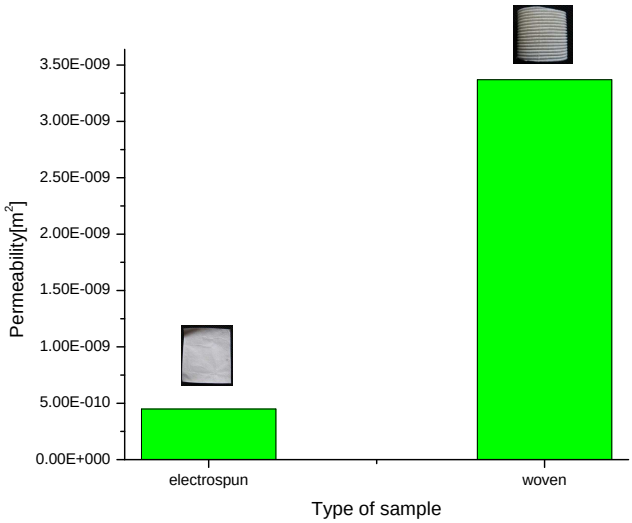

Figure 3.5.8: Experimental permeability [m^2] values according to equation 3.2.4 for woven and electrospun samples. The thickness and porosity were 0.9474 mm and 71.99% for the electrospun sample and 0.491 mm and 80.89% for the woven sample.

Once hydraulic conductivity was obtained, permeability was calculated based on equation 3.2.4, see Fig. 3.5.8. The difference between the electrospun and woven samples is probably related to the complex micro-structure of the electrospun sample that was observed by SEM, producing a greater resistance to pass through the textile wall.

3.5.3.2 Computational Method

Then, simulations were performed with the woven and electrospun virtual models in order to calculate permeability according to the methodology presented in section 3.2.2. Thickness and porosity were 1 mm and 96.68% for the electrospun virtual model and 0.45 mm and 82.58% for the woven virtual model. Although the porosity in the electrospun sample was greater than the woven sample, the electrospun micro-structure was more complex, causing greater resistance to the flow and lower permeability values, Fig. 3.5.9. This influence of the micro-structure possibly affects the mass transport and its ability for cells and nutrients to penetrate the wall.

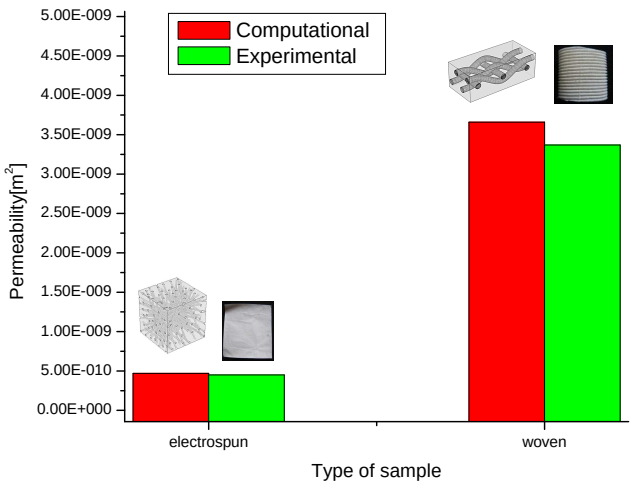

Figure 3.5.9: Experimental permeability [m^2] values according to equation 3.2.4 and computational permeability [m^2] values for woven and electrospun samples.

On the other hand, comparing experimental and computational data, it is possible to observe that the results have the same trend within a similar range, with a relative error of 4.65% for the electrospun sample and 8.53% for the woven sample, Fig. 3.5.9 and Table 3.2. The discrepancies between experimental and computational results can perhaps be attributed to slight differences in the unit cell micro-structure dimensions.

Table 3.2: Relative error of the permeability for woven and electrospun samples by experimental and computational methods.

	woven	electrospun
Simulation	3.66e-9	4.70e-10
Experimental	3.37e-9	4.49e-10
Relative error [%]	8.53	4.65

Lastly, another test case was done using a simplified unit cell with the same geometry, to examine how porosity affects permeability, Fig. 3.5.10. In this case, the yarn diameter was varied from 0.2 to 0.4 mm. From the geometric models, the porosities and permeabilities were calculated and are listed in Table 3.3.

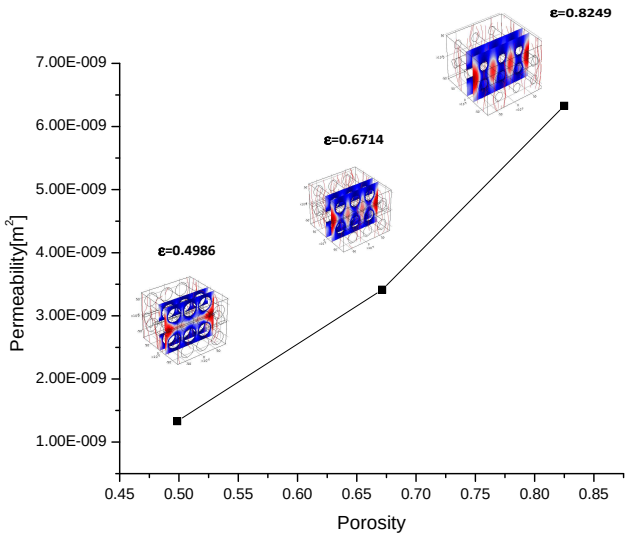

Figure 3.5.10: Predicting permeability for a simplified unit cell. Velocity distribution for three unit cells with different porosities.

As previously indicated , permeability is a parameter that measures the ability of a porous medium to conduct fluid flow and it depends on the geometry, porosity, pore size, among others [31]. The plot of the Fig. 3.5.10 shows that permeability increases as porosity is increased for the same geometry, possibly due to the fact that it offers less resistance to flow.

Table 3.3: Geometric parameters, porosities, and permeabilities for model of Fig. 3.5.10.

Yarn diameter [mm]	Pore size [mm]	Porosity[%]	Ave. Velocity [m/s]	Ave. Shear Stress [dyne/cm^2]	Reynolds	Permeability [m^2]
0.2	0.3	82.49	0.0018	0.6562	0.5475	6.3277e-9
0.3	0.2	67.14	0.0008	0.3883	0.2954	3.4134e-9
0.4	0.1	49.86	0.0003	0.1873	0.1152	1.3308e-9

3.5.4 Numerical Cases

The aim of these numerical cases is to study the flow pattern and the fluid-particle interaction for both the macro-domain and the micro-domain. For the macro-domain (i.e., a straight tubular structure with porous walls), the effect of parameters as the permeability, porosity and the duct-diameter were analyzed. For the micro-domain (i.e., woven and electrospun virtual models), the effect of the type of textile fabric was analyzed. The velocity field and particle residence index (PRI) are computed. PRI is an indicator used to measure how long a group of particles remains in a zone.

3.5.4.1 Macro-Scale: Straight Tubular Structure with Porous Walls

Effect of Permeability, Porosity and Duct Diameter on Local Fluid Dynamics The velocity profile for the macro domain, described in Fig. 3.3.2 along a vertical cross section in the middle of the duct, is depicted in Fig. 3.5.11. The plot shows a parabolic profile with the existence of radial velocity gradients across the interface between the porous wall and the free duct. It also shows that the axial flow rate in the duct is reduced as permeability is increased, Fig. 3.5.12. This behavior occurs for both diameters. Moreover, there is also a slight variation when porosity is modified. In general, this behavior indicates the tendency of the fluid to move towards the porous walls because of leakage flow, causing deviations from Poiseuille flow.

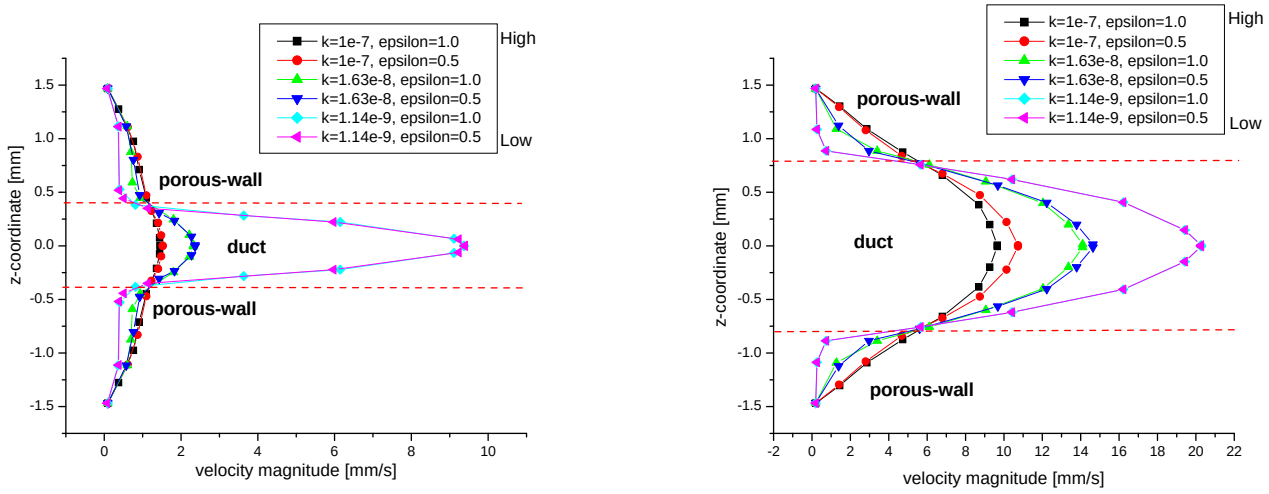

Figure 3.5.11: Cross section of velocity field (velocity magnitude in mm/s) in the middle of the duct with different radius, permeabilities and porosities. a) Radius=355um; b) Radius=900um

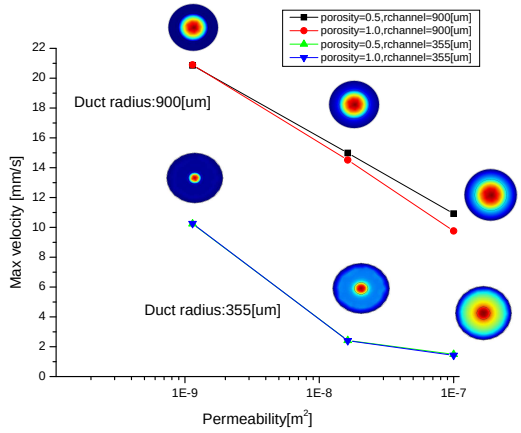

Figure 3.5.12: Maximum velocity [mm/s] versus permeability [m^2] of the wall with different radius, permeabilities and porosities. X-axis is in $\log_{10}$. Contours of the velocity magnitude corresponding to a cross section in the middle of the duct.

The hemodynamic conditions inside the textile graft lead to the development of superficial stresses near the wall due to blood flow. Usually, a linear shear stress curve characterizing Poiseuille flow is obtained for a Newtonian fluid in tubular vessels. However, porous walls cause different local characteristics as shown in Fig. 3.5.13 and Fig. 3.5.14. It shows that shear stress is reduced as permeability is increased. As mentioned before, the presence of low shear stress is frequently associated by stagnant points and can induce an excessive deposition of platelets over the wall.

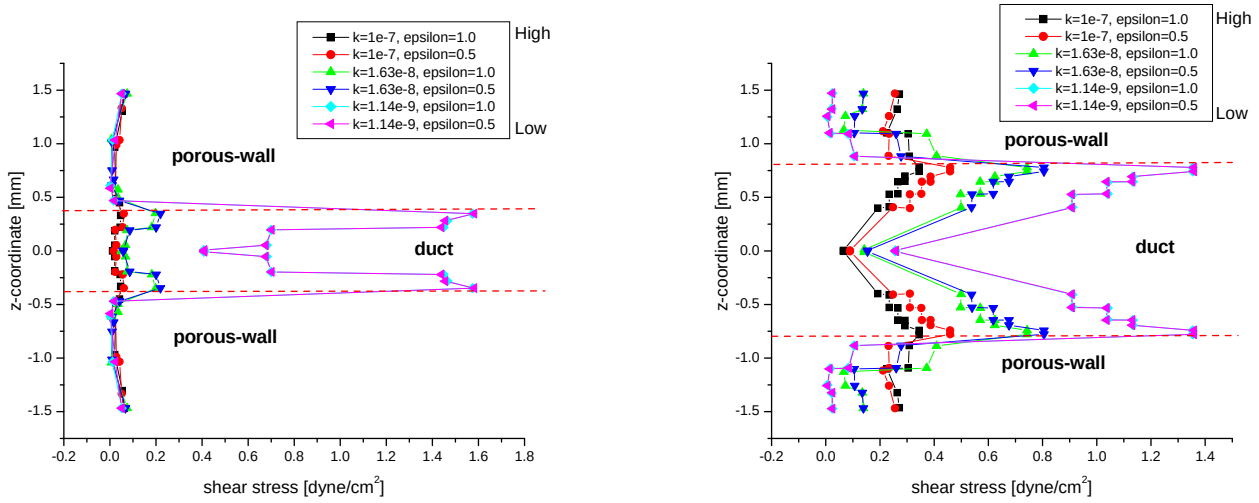

Figure 3.5.13: Cross section of the shear stress (in dyne/cm^2) in the middle of the duct with different radius, permeabilities and porosities. a) Radius=355um; b) Radius=900um.

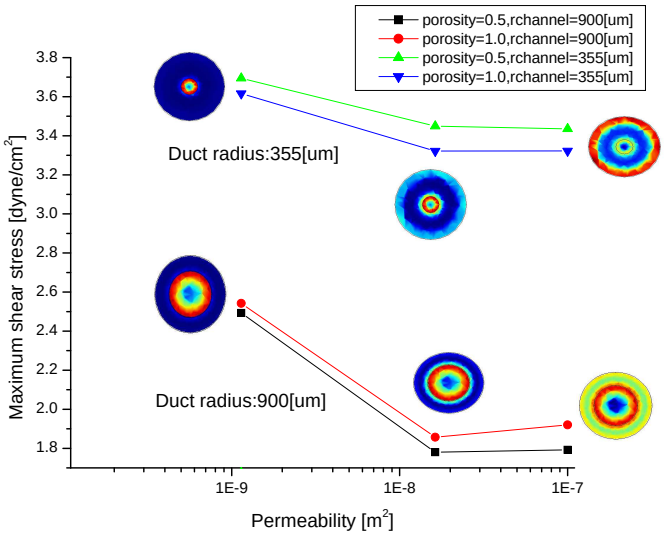

Figure 3.5.14: Maximum shear stress [dyne/cm^2] versus permeability [m^2] with different radius, permeabilities and porosities. X-axis is in $\log_{10}$. Contours of shear stress corresponding to a cross section in the middle of the duct.

Effect of Permeability, Porosity and Duct Diameter on Cellular Transport A total of 1000 particles were initially released at t=0. The first particles reached the outlet at around 3 seconds. The wall with high permeability (i.e, 1e-7m^2) had a PRI of 85.7 percent, i.e., number of deposited particles inside the wall divided by the total number of initially released particles, Fig. 3.5.15. On the contrary, the wall with low permeability (i.e., 1.14e-9m^2) had a PRI of 41.2 percent. With leakage flow through the porous wall, the particles move to the wall, increasing the residence time. This fact would increase the probability of platelet deposition and aggregation inside the wall.

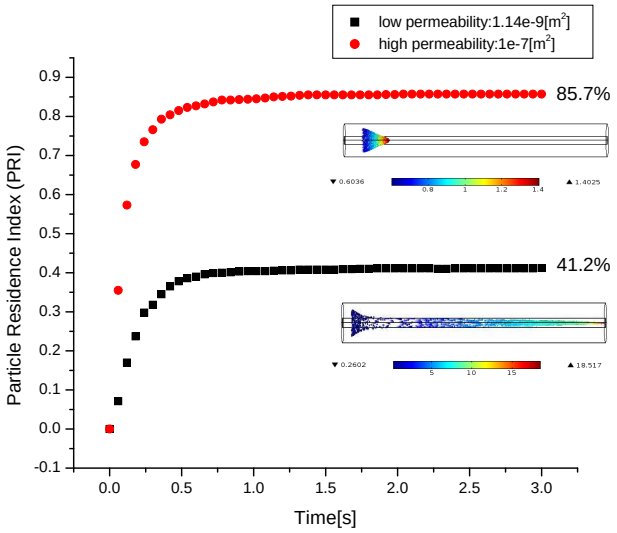

Figure 3.5.15: Time evolution of PRI in the porous wall (i.e., number of deposited particles inside the wall divided by the total number of initially released particles). Duct radius is 355 [um]. Particles were visualized for 3 seconds. The color scale represents the magnitude of particle velocity in mm/s.

For the case of the duct with radius of 900 um, the wall of high permeability (i.e., 1e-7m^2) had a PRI of 24.7 percent, while the wall of low permeability (i.e., 1.14e-9 m^2) had a PRI of 0 percent, Fig. 3.5.16.

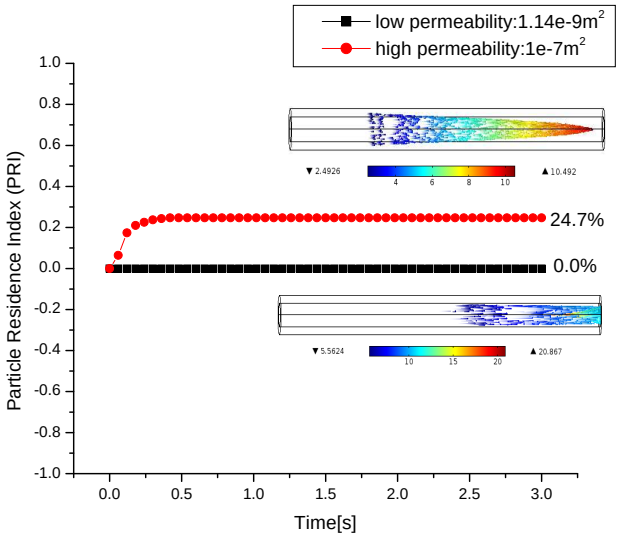

Figure 3.5.16: Time evolution of PRI in the porous wall (i.e., number of deposited particles inside the wall divided by the total number of initially released particles). Duct radius is 900 [μm]. Particles were visualized during 3 seconds. The color scale represents the magnitude of the particle velocity in mm/s.

3.5.4.2 Micro-Scale: Woven and Electrospun Samples

Effect of the Type of Textile Fabric Simulations were initially carried out for a unit cell of woven sample. The unit cell is composed of perpendicular yarns aligned along the x and y axes, which are interwoven to form a woven fabric. A normal pressure gradient of 1Pa/m was applied to the plane of the fabric (in the z-direction) and fluid flow was simulated through the unit cell. The pressure gradient was selected to set the flow in low Reynolds number regime. Moreover, periodic boundaries were used in the other directions, equivalent to simulating flow through an infinite fabric. As shown in Fig. 3.5.17, plane sections I, III and V represent the flow which is blocked by the yarns. Plane sections II and IV represent planes located between two lines of yarns and show lower flow resistance, where the flow has a direct path through the wall. As a result, this significant flow between two adjacent yarns define a high permeability zone. The top and bottom walls of the yarns are a favorable area for cells to adhere due to the lower flow velocity levels. In contrast, there are relatively high local velocities between two strands of yarns, so the cells would have more likelihood to be washed out the wall.

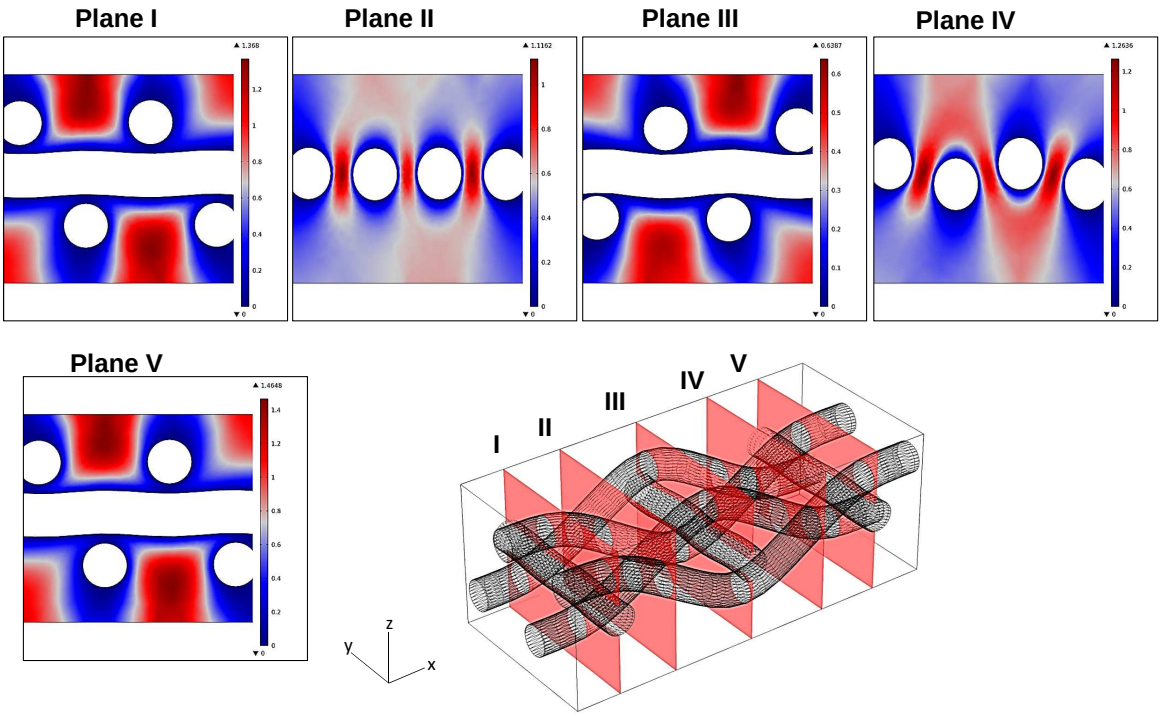

Figure 3.5.17: Velocity magnitude for five cross-sections at different locations within the unit cell of the woven sample. The color red indicates high velocity and blue low velocity. Velocity range is from 0.0 to 1.368 mm/s. The porosity of the woven fabric is 0.8258 and permeability is 1.14e-9 [m^2]. The applied pressure gradient drives the flow in the z-direction.

On the other hand, the porous structure in the electrospun sample is complex, and complicated flow patterns are observed as shown in Fig. 3.5.18. The velocity magnitude is higher in the narrowest pores and tends to decrease where the pore channel size increases. Moreover, there is a considerable zone with low flow velocity levels, possibly because of the increase of the pore path (tortuosity) and implying that this area would be suitable for cell attachment and deposition, Fig. 3.5.18 (plane sections II and III). However, plane sections I and IV have a larger pore size with low resistence to flow (i.e., high permeability).

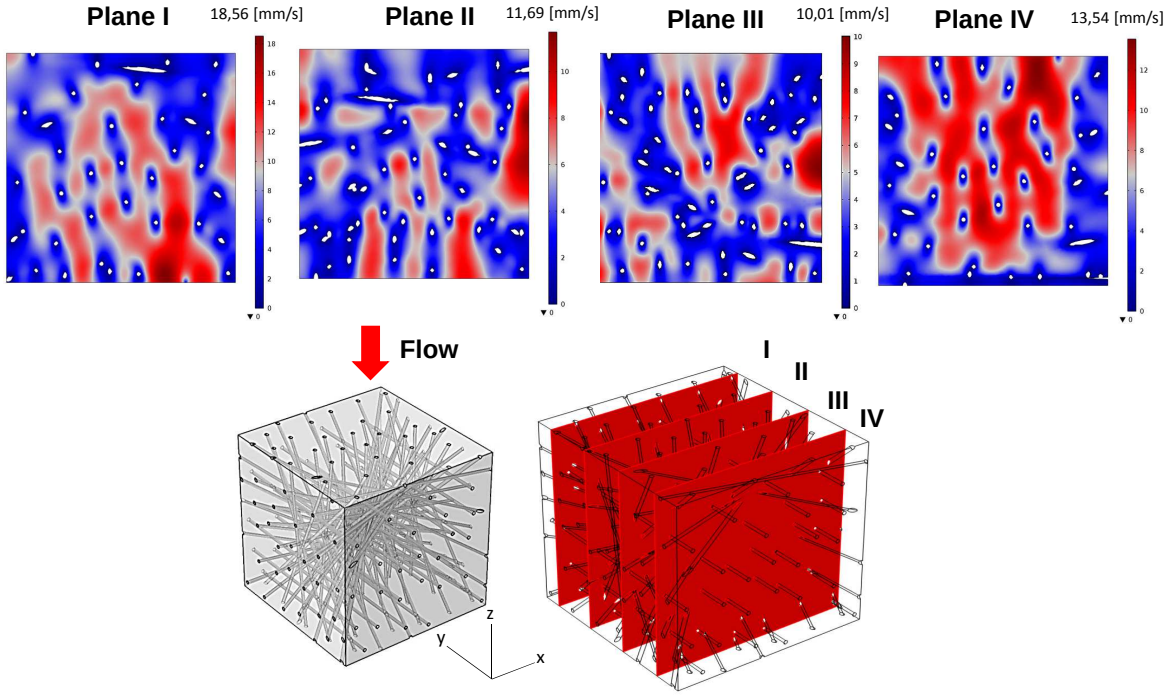

Figure 3.5.18: Velocity magnitude [mm/s] for four cross-sections at different locations within the unit cell of an electrospun sample. The color red indicates high velocity and blue low velocity. Velocity range is from 0.0 to 18.516 mm/s. The electrospun porosity is 0.9668 and the permeability is 4.7012e-10 [m^2]. The applied pressure gradient drives flow in the z-direction. .

Table 3.4 summarizes some of the properties of the samples studied and their computational results: average velocity [mm/s], average shear stress [dyne/cm^2] and permeability [m^2] values. Although the electrospun sample has higher porosity values than the woven sample, its microstructure is more complex with higher surface area values, causing lower values of permeability and higher values of particle residence index, Fig. 3.5.19. A total of 3000 particles were initially released at t=0.

Table 3.4: Properties and computational results of the samples studied: porosity, specific surface area, average velocity, average shear stress and permeability.

Sample	Porosity	Specific surface area [mm^2]	Average velocity [mm/s]	Average shear stress [dyne/cm^2]	Permeability [m^2]
woven	0.8258	2.55	0.7251	0.5156	1.14e-9
electrospun	0.9668	1243.3	4.6525	0.3265	4.7012e-10

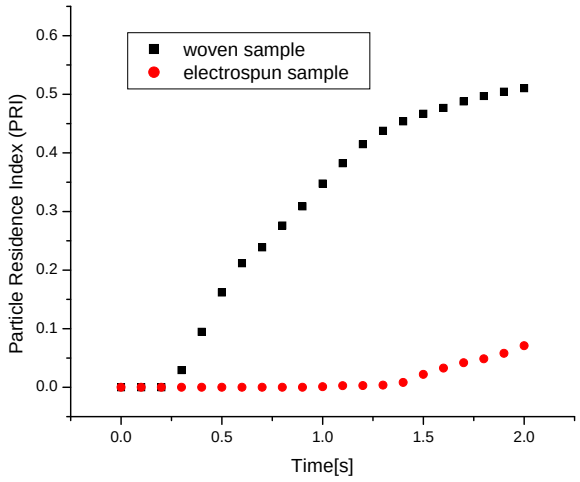

Figure 3.5.19: Particle Residence Index (PRI) for woven and electrospun samples in the outlet side. The PRI for this case is defined as the ratio of the number of particles which reach the outlet divided by the number of particles released. A total of 3000 particles were initially released at t=0.

The electrospun sample presents higher PRI values than the woven sample. This means that is more likely for the electrospun sample that the cells remain trapped increasing the agregation and deposition of platelets, Fig. 3.5.20 and 3.5.21.

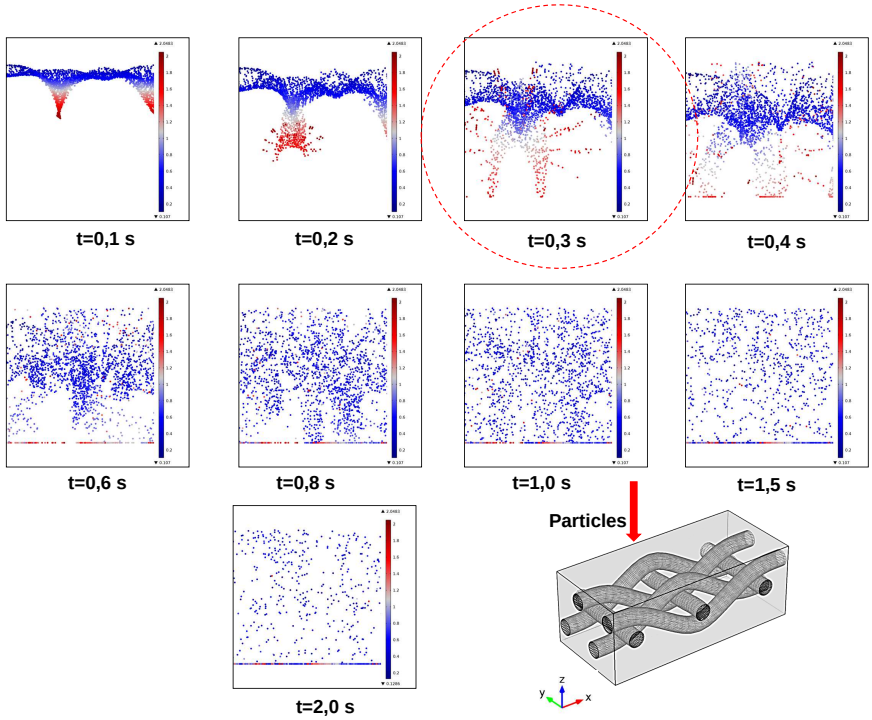

Figure 3.5.20: Plot of particle trajectories inside the woven wall. The color red indicates high particle velocity and blue low particle velocity. Particle velocity range is from 0.0 to 2.0483 mm/s. The circle highlights the number of particles which reach the outlet at 0.3s.

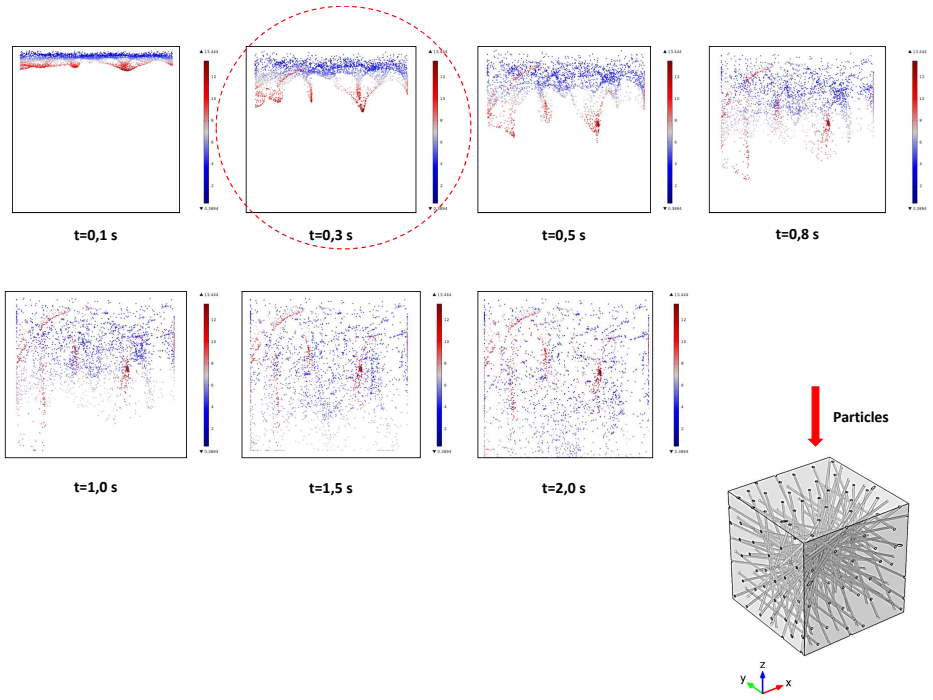

Figure 3.5.21: Plot of particle trajectories inside the electrospun wall. The color red indicates high particle velocity and blue low particle velocity. Particle velocity range is from 0.0 to 13.44 mm/s. The circle highlights the number of particles that do not reach the outlet at 0.3s.

The flow pattern and fluid-particle interaction of individual particles with platelet-like properties have been described for both macroscopic and microscopic viewpoint. The effect of two different type of fabrics, electrospun and woven, was evaluated at several length scales considering the pass of fluid and the transport of particles through the porous walls. The next chapter presents the implementation of a numerical case that includes one of the main applications of textile vascular grafts to repair Abdominal Aortic Aneurysms (AAA).

Chapter 4

MODELLING OF A TEXTILE ENDOVASCULAR GRAFT IN AN ANEURYSM WITH CLOT FORMATION

4.1 Introduction

One of the main applications that are treated by vascular grafts are aneurysms [87]. An aneurysm is an abnormal irreversible bulging of an artery [25, p.278]. This cardiovascular health disease is the 13th leading cause of death in the United States, i.e., about 15.000 deaths every year [80, 25, p.279]. Most aneurysms occur in the major vessels (specially, in the abdominal aorta below the renal arteries), where the walls of the affected vessel are weak and can rupture with a potentially fatal outcome. Some causes are due to tissue degeneration, trauma, congenital defects and microbial attack, among others. There are several implications from a fluid mechanics viewpoint, producing unusual flow characteristics like large vortices near the wall and stagnation points. As was mentioned before, stagnation points may increase the likely of thrombus formation in the bulge region [22, p.251]. Moreover, a blood clot may travel and block distal sites (i.e embolism), such as the foot, producing an ischemic condition known as a *blue toe*.

Vascular grafts is one of the treatments to prevent rupture from abdominal aortic aneurysms (typically Woven Dacron® grafts), restoring the normal blood flow and shielding the weakened aneurysm wall [25, p.283]. Anastomosis is the surgical procedure to join two blood vessels using a graft. This procedure can be in two ways: open surgery and surgery with a catheter delivery system via the femoral and iliac arteries [44, 40], Fig. 4.1.1.

Additionally, there are two common configurations to replace the diseased arterial segment: end-to-end and end-to-side anastomoses, Fig. 4.1.2. The anastomoses usually used to repair an abdominal aortic aneurysm are placed in an end-to-end fashion [22, p.317].

Although the textile vascular grafts have been used and studied since the 1960s [87], this tech-

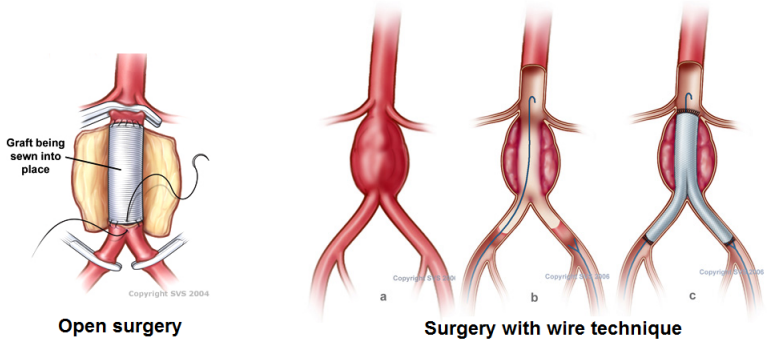

Figure 4.1.1: Anastomosis: Open Surgical Aneuysm Repair (left) and Endovascular Stent Graft (rigth). Figure taken from Vascular Web[38]

nology still suffers from several limitations like the formation of clots over its artificial surface [83, 65]. One of the possible reasons of graft thrombosis may be due to the body's response to the implantation of a foreign material for the lack of endothelium [22, p. 322]. This failure is more likely to occur in regions of static or slow flow where the tendency for clotting is enhanced. Additionally, thrombus formation depends on the residence time, specially in areas with high platelet-wall interactions [22, 25, p.403,p.246].

The vascular grafts have a finite life span which is usually reported based on patency data [19]. The patency is the ability to remain open and is reported in a percentage. A value of 100% is a totally open lumen. The patency can begin to fall by thrombosis in the early postoperative period of 1 month. When an artificial wall of the graft is first exposed to blood, a process of activation, adhesion and aggregation of platelets will begin, which may form a platelet plug that occludes the graft. Occlusion of a graft often results in hospital re-admission and re-operation for the patient. This clot will narrow the lumen volume acting as an obstacle to the flow and causing a restriction in blood supply to the textile wall, needed for tissue repair, or a distal ischemia on the downstream. Hence, the presence of clots may alter the physiological transport and the local environment of the graft, reducing the flow and may lead to graft occlusion [87].

Whereas several studies have concentrated on understanding only the biochemical process of thrombus formation [72, 51], there is a lack of models which are able to show graft occlusion through the transport and deposition of individual platelets over the artificial wall of textile vascular grafts [83, 94].

The aim of this chapter is to model the flow pattern and the fluid-particle interaction, which include activation, aggregation and adhesion of platelets in a duct with an aneurysm geometry and the presence of a textile vascular graft. For this issue, the artificial wall of textile graft is defined with a fictitious domain model and evaluated with different porosities. The fluid-particle interaction is in two and four-way coupling.

This model may improve the understanding of the flow behaviour in an abdominal aortic aneurysm, including the wall of a textile graft with different porosities via a non-invasive com-

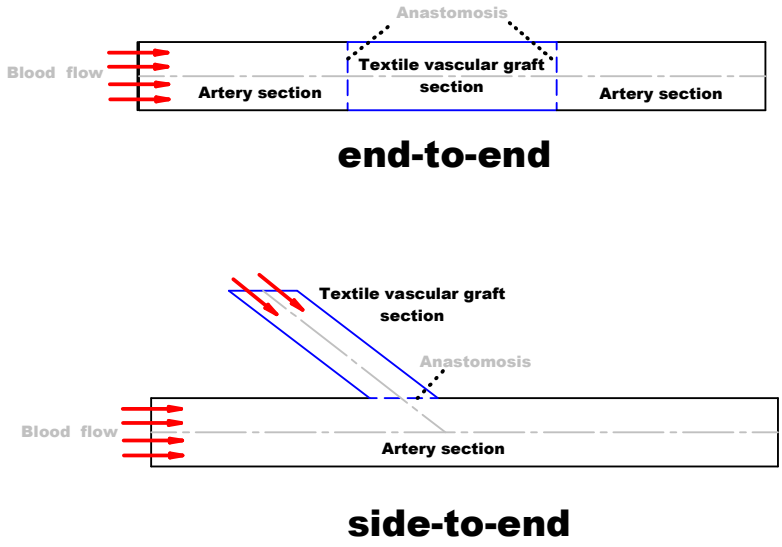

Figure 4.1.2: Common configurations to replace a disease segment of artery: end-to-end and end-to-side (bypass). [97]

putational methodology.

4.2 Methods

A set of two numerical cases is described in this section. The aim of these cases is to model the flow pattern and the fluid-particle interaction, which include activation, aggregation and adhesion of platelets, related with the graft occlusion. Two domains are considered with the presence of a textile vascular graft: a duct with an idealized aneurysm geometry and a fusiform infrarenal aneurysm based on a Magnetic Resonance Angiography (MRA) image. This issue involves one of the main applications of textile vascular grafts to repair Abdominal Aortic Aneurysms (AAA), where the anastomoses are placed in an end-to-end fashion. Furthermore, the artificial wall of the graft, that forms a barrier between the blood and the aneurysm, is defined with a fictitious domain model and is evaluated with different porosities in a range from 0.6 to 1.0, in order to consider the effect both on local fluid dynamics and on fluid-particle interaction among platelets. The fluid-particle interaction is defined in two and four-way coupling. Lastly, a code is implemented on a Finite Element solver like FreeFem [1] and Paraview software is used for the post-processing of the results.

4.2.1 Geometry and Boundary Conditions

4.2.1.1 Duct with an Idealized Aneurysm Geometry

Textile vascular grafts in Dacron® are commonly used in large arteries to repair Abdominal Aortic Aneurysms (AAA), where the anastomoses are placed in an end-to-end fashion [87]. The domain Ω for this case is shown in Fig. 4.2.1. The geometry of the duct is defined with an internal diameter of 2 cm, a length of 20 cm and a textile wall thickness of 0.2 cm. The expansion geometry in the aneurysm region is defined with a sinusoidal function and a length of 4 cm. Fluid is injected into the duct at x=0 having a uniform velocity profile (inlet) with a value of 0.2 m/s, which is representative of the mean flow for resting conditions in the abdominal aorta (laminar blood flow) [80]. Furthermore, a free stress condition is used at the outlet and a no-slip condition at the walls. A total of 327 particles are initially released at t=0. After establishing the numerical results to be independent of mesh density, the final mesh consisted of 2776 triangular elements and 1509 nodes within 5% relative error.

(a)

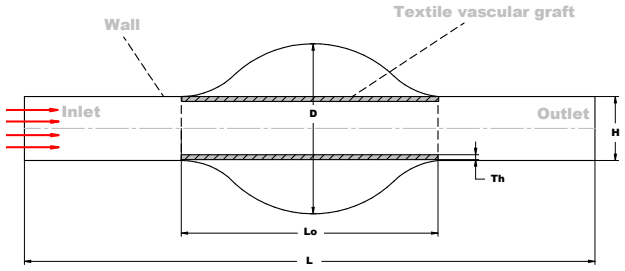

(b)

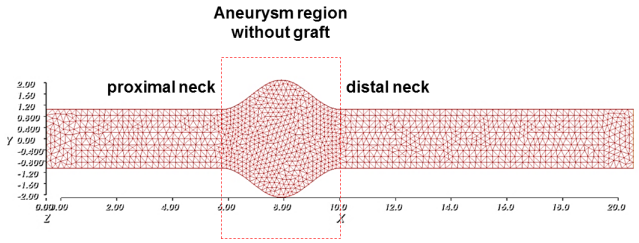

Figure 4.2.1: a) Scheme of a duct with an expansion region like an ideal fusiform aneurysm. b)Final mesh with 2776 triangular elements and 1509 nodes. The geometry of the duct is defined with an internal diameter of 2 cm and a length of 20 cm. The expansion geometry in the aneurysm region is defined with a sinusoidal function and a length of 4 cm.

4.2.1.2 Processing a MRA Scanned Image of an Infrarenal Aneurysm and Model Reconstruction

The next case considers the computational geometric reconstruction of a more realistic 2D domain of an fusiform aneurysm. The reconstruction was developed based on a Magnetic Resonance Angiography (MRA) image of an infrarenal aneurysm [74]. Image processing filters were used to extract the aneurysm morphology, to smooth the image, reduce the noise and detect the edges in the original image, Fig. 4.2.2. ImageJ® software [2] was used for this purpose. A thresholding method was used for image segmentation in regions with similar greyscale in order to create a PGM image (i.e. Portable Gray Map) which can be read by FreeFem++ [1]. The advantage of obtaining first a binary image is that it reduces the complexity of the image and simplifies the process of edge detection. Later, the discretization of an isoline was obtained in order to detect the boundaries of the domain and to construct the mesh, which is a direct input for the fluid solver.

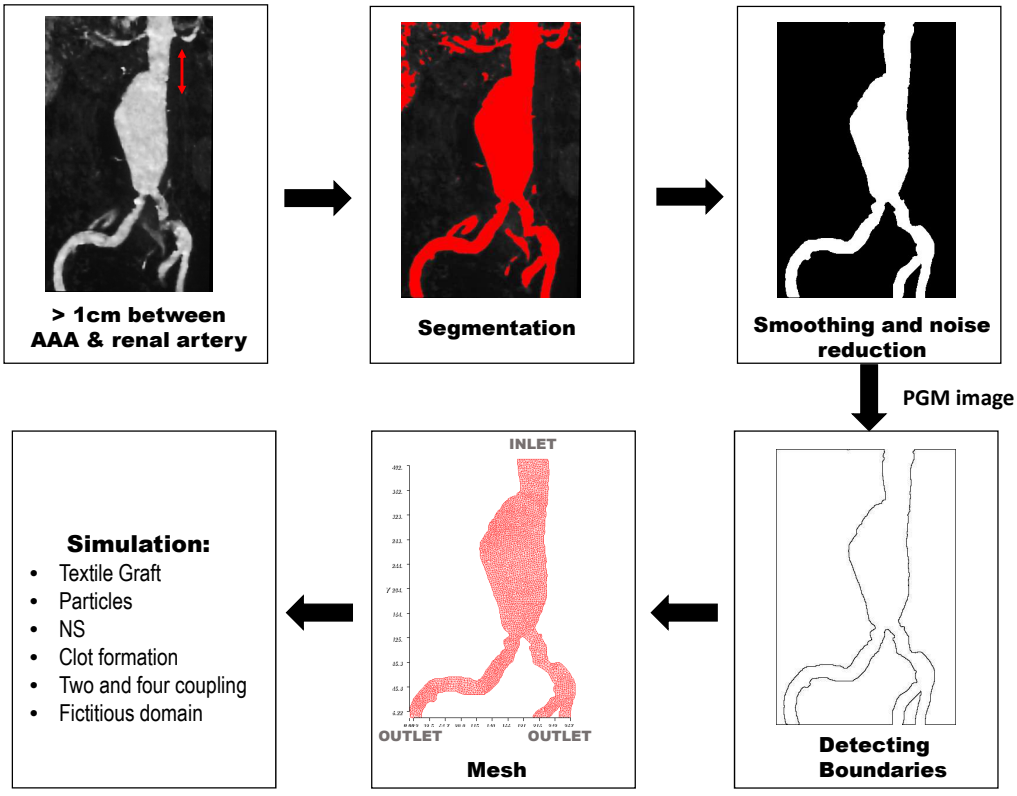

Figure 4.2.2: Image processing steps from original image of an infrarenal aneurysm based on a Magnetic Resonance Angiography (MRA) to mesh, which is a direct input for the fluid solver. The final mesh without graft consisted of 9502 triangular elements and 5052 nodes.

The inlet and outlet diameter were 2.65 cm and 1.18 cm, the maximum aneurysm diameter was 5.9 cm, and the length of the aneurysm region was 13.45 cm. As in the previous case, a uniform flow was assigned at the inlet with a value of 0.2 m/s, a free stress condition at the outlet, and a no-slip condition at the walls. A total of 524 particles are initially released at t=0. Lastly, after

establishing the independence in mesh size, the final mesh consisted of 9502 triangular elements and 5052 nodes within 5% relative error.

4.2.2 Governing Equations

4.2.2.1 Clot Formation Model

One aspect to consider is the blood-material interaction between platelets and the artificial surface of the graft wall [37]. The platelets particles can be in two states: passive or active. The passive state is a normal state of platelets following the flow without any interaction with other platelets. When a passive platelet comes close to the artificial wall of a textile graft, it becomes active and two external forces, adhesion and aggregation, gradually increase. Then, the activated platelets are aggregated to other activated platelets, forming a primary thrombus. To incorporate this adhesion force in the third term of the equation 3.3.7, an attractive (bonding) force is introduced within a distance d_{ad}, connecting a platelet particle i to a particle j joined to the wall [48, 71]:

$$\vec{f}_{ad} = \begin{cases} k_{ad}(\mid \vec{r}_{ij} \mid -r_o)\hat{n}_{ij} & \text{if } \mid \vec{r}_{ij} \mid \leq d_{ad} \\ 0 & \text{if } \mid \vec{r}_{ij} \mid > d_{ad} \end{cases} \tag{4.2.1}$$

The platelet aggregation is initiated by placing one activated platelet attached to the wall. The aggregation force $\vec{f}_{ag}$ acts among activated platelets within a distance d_{ag} and can be expressed as:

$$\vec{f}_{ag} = \begin{cases} k_{ag}(\mid \vec{r}_{ij} \mid -r_o)\hat{n}_{ij} & \text{if } \mid \vec{r}_{ij} \mid \leq d_{ag} \\ 0 & \text{if } \mid \vec{r}_{ij} \mid > d_{ag} \end{cases} \tag{4.2.2}$$

where k_{ad} and k_{ag} are constants proportional to the forces, $\hat{n}_{ij} = \vec{r}_{ij} / \mid \vec{r}_{ij} \mid$ is the vector between the platelet particles i and j, and r_o is the length among particles without overlapping, Fig. 4.2.3.

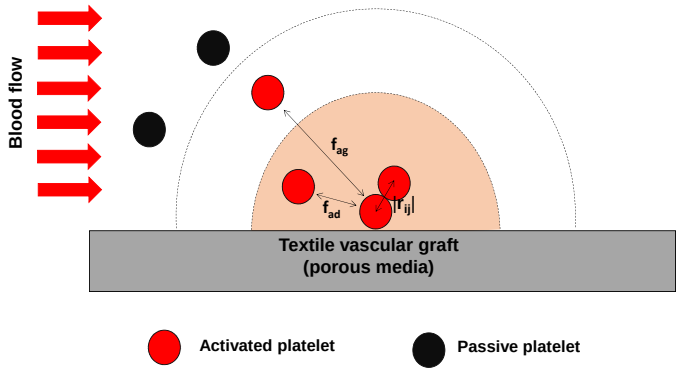

Figure 4.2.3: Model of platelet aggregation and adhesion. The scheme has been modified from [48]. If a passive platelet comes close to the artificial wall of a textile graft, it becomes active and two external forces, adhesion and aggregation, gradually increase.

4.2.2.2 Two and Four-Way Coupling

As was mentioned before, blood is a concentrated suspension of cells in a complex aqueous solution [25]. The process of activation, adhesion and aggregation of platelets lead to the formation of a primary thrombus, acting as an obstacle to the flow. In this case, particle-to-fluid forces are transferred to the fluid as an additional body force in the momentum equation [67, 89]:

$$\rho \frac{\partial \vec{u}}{\partial t} + \rho \vec{u} \cdot \nabla \vec{u} = -\nabla p + \mu \triangle \vec{u} + \vec{F} \tag{4.2.3}$$

where $\vec{F}$ is a source term due to the influence of the particles on the fluid. This is known as a two-way coupling and $\vec{F}$ can be defined as [67, 89]:

$$\vec{F} = \frac{1}{n_f} \vec{f}_d^{pf} \text{ with } d = 1..n_s \tag{4.2.4}$$

where n_s is the number of space dimension ($n_s = 2$ for 2D problems), $\vec{f}_d^{pf}$ is the contribution of all the particles belonging to an element of the fixed mesh, and n_f is the fluid volume fraction defined as:

$$n_f = 1 - \frac{1}{A_{element}} \sum_{j=1}^{n_j} A_j \tag{4.2.5}$$

where n_j is the number of particles contained in an element, $A_{element}$ is the area of an element of the mesh, and A_j is the area of the jth particle. Moreover, particle-particle interaction can be taken into account for the clot formation model. This is called four-way-coupling.

4.2.2.3 Fictitious Domain Model

In order to simulate porous regions immersed in fluid domains, several non-boundary fitting methods can be used [96, 43]. One of them is the Brinkman penalization method [13, 49], adding the Brinkman penalization term $\alpha\mathbf{u}$ to the Navier-Stokes equations. This term represents the effect of the no-slip boundary condition and may be used to define the boundaries between the fluid and the textile wall in a fixed grid, Fig. 4.2.4. The main advantage of the fictitious domain approach for porous media problems is that it can use the same fixed Cartesian grid instead of body-conformal grids, that usually needs be re-generated at each time step.

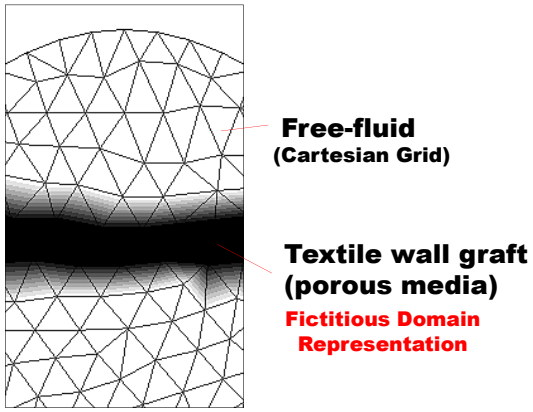

Figure 4.2.4: The artificial wall is defined with a fictitious domain model and different porosities in order to simulate the porous region immersed in fluid domain.

The Brinkman penalization parameter α can be defined as inverse permeability of the medium where the fluid moves [18]:

$$\alpha(\rho) = \alpha_{max} + (\alpha_{min} - \alpha_{max})\rho\frac{1+q}{\rho+q} \tag{4.2.6}$$

where ρ is a density function over the entire domain with $0 \leq \rho \leq 1$ and q is a penalization parameter (as it is smaller, the α is more penalized). By definition, ρ is equivalent to the porosity of the wall and takes a value of 1 for an open fabric and 0 for a fabric with no open spaces. Therefore, the value of α coefficient has a high value in a solid region (i.e., α_{max}), causing the velocity to tend to zero, and it has a low value in a fluid region (i.e., α_{min}). Both terms are defined as follows [18]:

$$\alpha_{min} = 2.5\mu/100^2 \approx 0 \text{ in fluid region} \tag{4.2.7}$$

$$\alpha_{max} = 2.5\mu/0.01^2 \approx \infty \text{ in solid region} \tag{4.2.8}$$

Lastly, representative AAA with a textile vascular graft are showed in Fig 4.2.5.

(a)

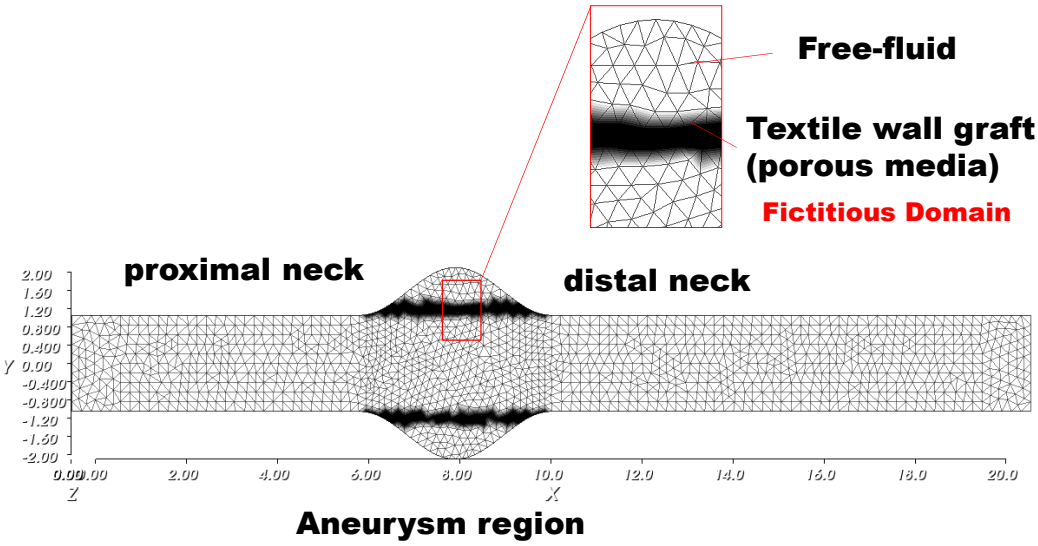

(b)

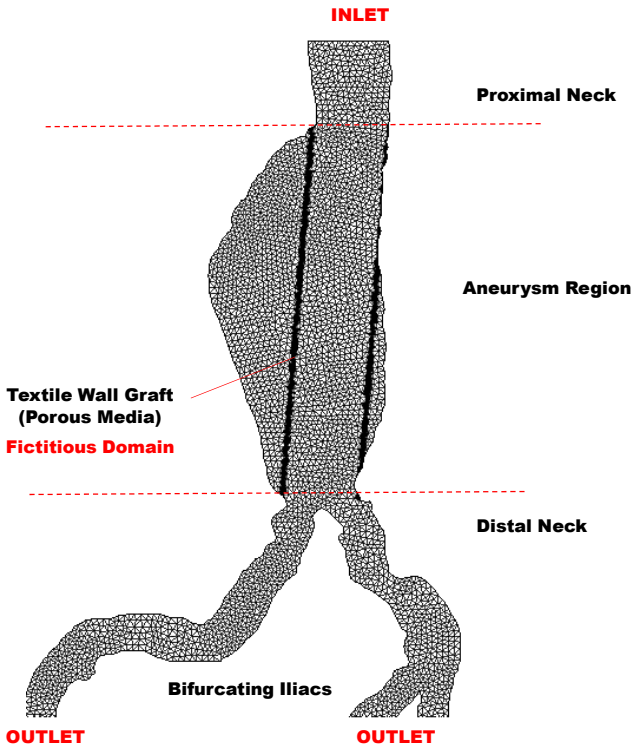

Figure 4.2.5: Representative AAA with a textile vascular graft: a) Duct with an expansion region like an ideal fusiform aneurysm and the presence of textile wall. b)Infrarenal fusiform aneurysm and the presence of textile wall.

4.2.2.4 Blood Flow Equations

The Lagrangian formulation in strong form for the incompressible fluid of those numerical cases solely use one system of equations in the whole domain and can be written as follows:

$$\frac{D\mathbf{u}}{Dt} = -\nabla p + \nu \triangle \mathbf{u} + \frac{1}{n_f}\mathbf{f}_d^{pf} + \alpha(\rho)\mathbf{u} \tag{4.2.9}$$

$$\nabla \cdot \mathbf{u} = 0 \tag{4.2.10}$$

where the forces $\mathbf{f}$ acting on the *ith* particle are the drag force, buoyancy and gravitational forces, aggregation and adhesion forces. In order to consider two-way coupling and to show the influence of primary thrombus on local dynamics fluid, the term $\frac{1}{n_f}\mathbf{f}_d^{pf}$ is computed for each particle and added to equation 4.2.9. Additionally, having supplied the scalar field $\alpha(\rho)$ for the fictitious domain between blood flow and the graft wall, the Brinkman penalization term $\alpha(\rho)\mathbf{u}$ is also added to the equation 4.2.9.

4.2.3 Numerical Implementation

Keeping the Finite Element method in mind , the momentum and mass balance equations are written in a weak form. Multiplying the fluid equations by test functions $v \in V = H_0^1(\Omega)$ and $q \in Q = \left\{q \in L^2(\Omega) : \int_\Omega q = 0\right\}$ and integrating by parts over Ω, the resulting integral expressions are:

Find $\mathbf{u} \in V$ and $p \in Q$ s.t.

$$\int_\Omega \tfrac{1}{dt}\mathbf{u}^{n+1}\mathbf{v}d\Omega - \int_\Omega \tfrac{1}{dt}\mathbf{u}^n(\mathbf{X}^n)\mathbf{v}d\Omega = \int_\Omega p\nabla\cdot\mathbf{v}\,d\Omega + \int_\Gamma(\tfrac{\partial\mathbf{u}}{\partial n})\mathbf{v}\,d\Gamma - \nu\int_\Omega \nabla\mathbf{u} : \nabla\mathbf{v}\,d\Omega + \ldots$$

$$\int_\Omega(\tfrac{1}{n_f}\mathbf{f}_d^{pf})\mathbf{v}\,d\Omega + \int_\Omega \alpha(\rho)\mathbf{u}\,\mathbf{v}\,d\Omega \qquad \forall\mathbf{v}\in V \tag{4.2.11}$$

$$\int_\Omega q\nabla\cdot\mathbf{u}\,d\Omega = 0 \quad \forall q \in Q \tag{4.2.12}$$

The Characteristics method is used to discretize the time derivative on a Lagrangian frame [70, 34] (see Appendix A). On the other hand, the transport of the particles is described based on the equation 3.3.7. Moreover, although there are different integration schemes, such as the Implicit Euler and the Leap-Frog, to describe the advance of each particle, Verlet-type algorithm is used to advance the set of positions and velocities of the particles using a global fixed time step [50], Table 4.1. According to literature [51], the Verlet scheme is stable and fast.

Table 4.1: The Verlet algorithm for describing the advance of each particle

$$step1: {}^{n}\vec{F}_i = {}^{n}\vec{F}_{i_{drag}} + {}^{n}\vec{F}_{i_g} + {}^{n}\vec{F}_{i_{ext}}$$
$$step2: \tilde{v}_i = {}^{n}\vec{v}_i + \frac{1}{2}\triangle t\, {}^{n}\vec{F}_i$$
$$step3: {}^{n+1}\vec{r}_i = {}^{n}\vec{r}_i + \triangle t\, {}^{n}\vec{v}_i + \frac{1}{2}(\triangle t)^2\, {}^{n}\vec{F}_i$$
$$step4: {}^{n+1}\vec{F}_i = \vec{F}_i({}^{n+1}\vec{r}, \tilde{v}_i)$$
$$step5: {}^{n+1}\vec{v}_i = \tilde{v}_i + \frac{1}{2}\triangle t\, {}^{n+1}\vec{F}_i$$

Lastly, a summary of the algorithm for this case is presented in Fig. 4.2.6. The algorithm was implemented with FreeFEM++ software and Paraview software was used for the post-processing of the results.

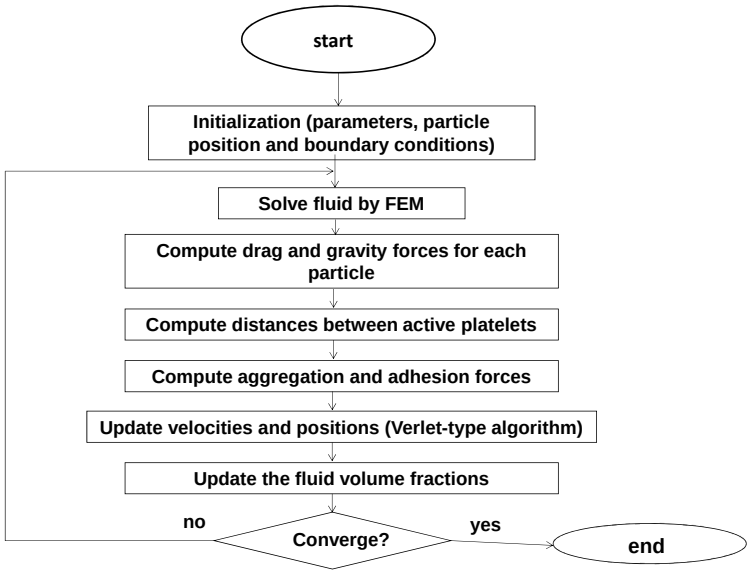

Figure 4.2.6: Algorithm summary: Finite Element Method and Particle based method.

4.3 Results and Discussion

The results of this section are divided into two groups: a duct with an idealized aneurysm geometry and an Infrarenal Aneurysm from Processing a MRA Scanned Image. For both cases, the velocity field, the number of particles adhered to the textile wall and the particle residence index (PRI) are computed varying the porosity of the textile wall.

4.3.1 Duct with an Idealized Aneurysm Geometry and the Presence of a Textile Graft

Figures 4.3.1 and 4.3.2 illustrate the transport of particles with platelet-like properties through a duct with an idealized aneurysm geometry and the thrombus formation at several time instants.

Marked variations of flow conditions were observed that deviated from Poiseuille-type flow with an open fabric (porosity=1.0) in the aneurysm region, Fig. 4.3.1. The flow was more disturbed and a slowly rotating vortex was observed, decelerating the velocity by around 24 percent with respect to the wall of porosity=0.6. This region of recirculation in the aneurysm region implies that the number of platelets colliding with the textile wall increases and can form small blood clots. Furthermore, the aneurysm with a textile wall of porosity=0.6, the blood flow is rather uniform with less leakage flow than the textile wall of porosity=1.0, Fig. 4.3.2. Hence, the presence of the textile wall reduces the circulation of blood and particles inside the aneurysmal cavity.

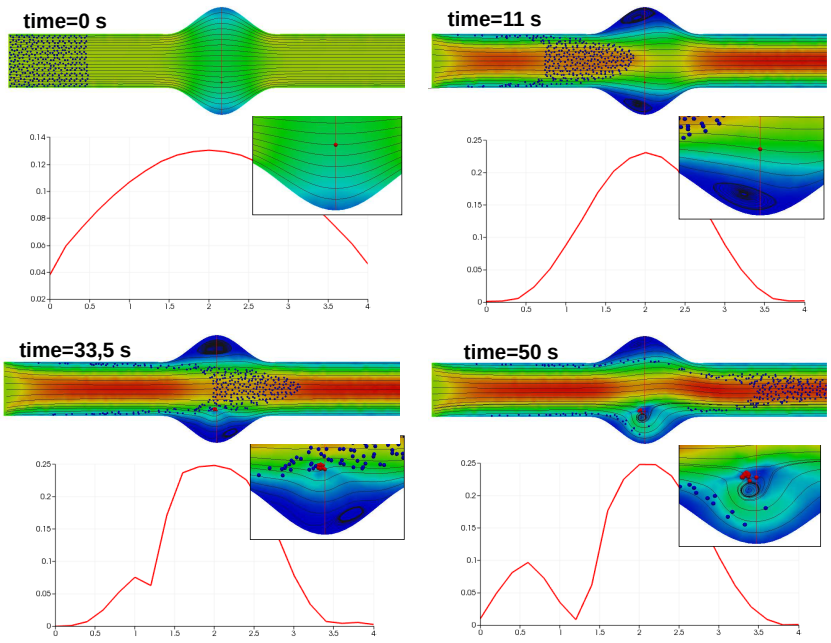

Figure 4.3.1: Duct with an idealized aneurysm geometry: distribution of particles and flow for different time instants and the presence of a textile wall of porosity 1.0. Platelet aggregation is initiated by placing one active platelet attached to the wall. The color shows the velocity magnitude in m/s .

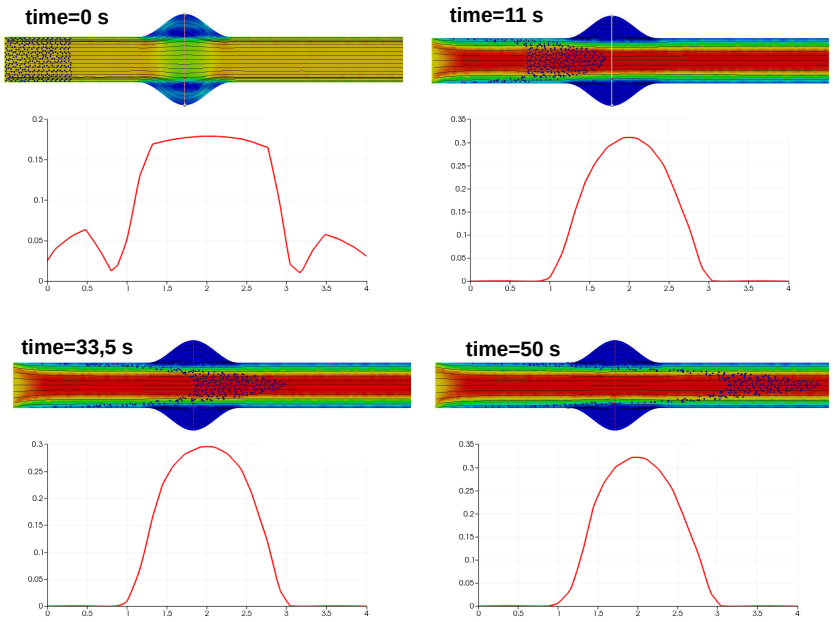

Figure 4.3.2: Duct with an idealized aneurysm geometry: distribution of particles and flow for different time instants and the presence of a textile wall of porosity 0.6 . Platelet aggregation is initiated by placing one active platelet attached to the wall. The color shows the velocity magnitude in m/s .

Figure 4.3.3 shows the number of platelets adhered to the textile vascular wall. The plot revealed that the growth rate was higher when the fabric was totally open (i.e., a porosity of 1.0) and was lower as the porosity was reduced. This behavior is likely due to the fact that the particles move to the center of duct when the porosity is lower.

Additionally, the aneurysm zone with an open fabric alters downstream and produces a slow flow with a susceptible place for particle deposition with longer particle residence times. The case with an open fabric, a PRI of 19.87 percent was observed after 50s, while a PRI of 13.46 percent was observed with the wall of porosity 0.6, Fig. 4.3.4.

4.3.2 Infrarenal Aneurysm Based on an MRA Image with the Presence of a Textile Graft

Figure 4.3.5 shows the flow pattern, the transport of particles and thrombus formation through an infrarenal aneurysm with the presence of a textile vascular graft at several time instants. The vortices, that develop and dissipate in the aneurismal cavity, travel downstream towards the distal neck and remain longer in the midsection, thus allowing the creation of stagnating flow. Vortex growth creates favorable conditions for increased platelet deposition and thrombus formation due to recirculating flow. This disturbed flow patterns can be attributed to the irregular geometry, curvature effects and branching. Furthermore, it was identified that thrombus formation has a strong impact on the flow field, defining a stagnation point and dividing streamlines which pass through this point.

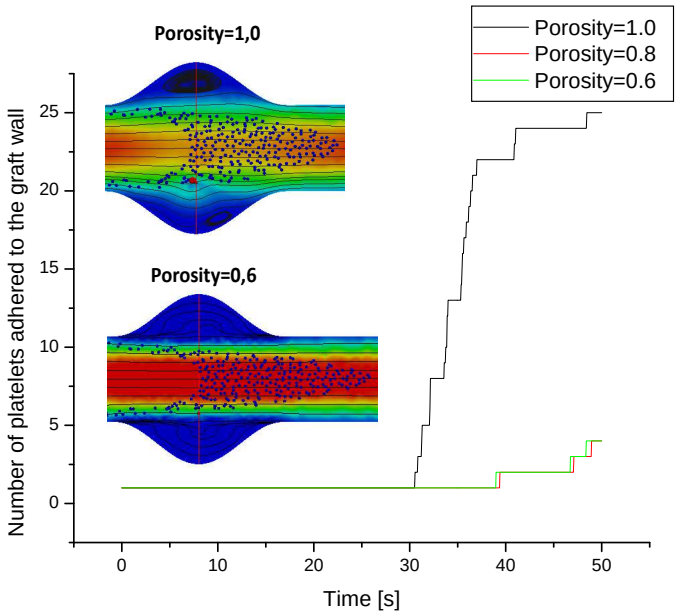

Figure 4.3.3: Number of platelets adhered to the graft wall. The results are shown with different porosities of the wall.

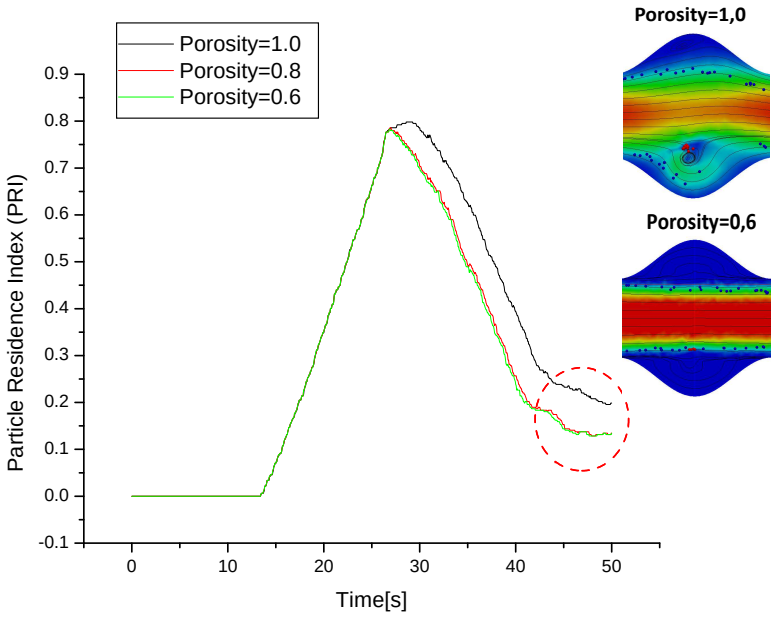

Figure 4.3.4: Time evolution of PRI in the aneurysm zone. The PRI for this case was defined as the ratio of the number of particles inside the aneurysm zone divided by the total number of initially released particles. The circle highlights a PRI of 19.87 percent for the open fabric (porosity=1.0) after 50s, while a PRI of 13.46 percent was observed with the wall of porosity 0.6

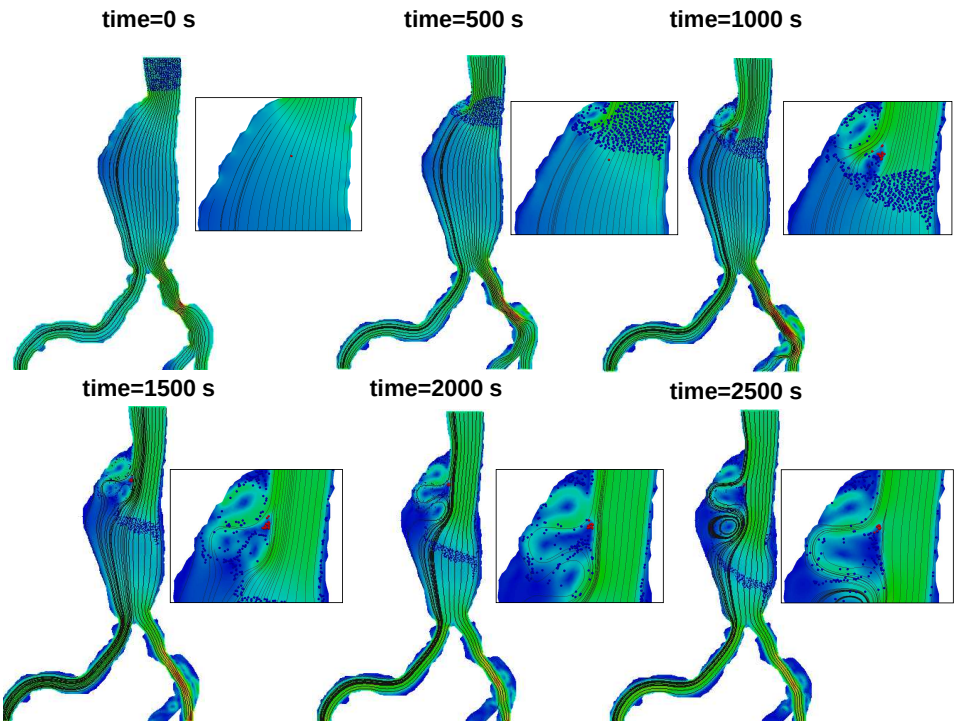

Figure 4.3.5: Infrarenal aneurysm based on an MRA image: distribution of particles and flow for different time instants. The porosity of the textile wall has a value of 1.0 (i.e. open fabric). The platelet aggregation is initiated by placing one active platelet attached to the textile wall near the proximal neck. The color shows the velocity magnitude in m/s.

Moreover, Fig. 4.3.6 shows a parallel flow to the textile wall and was weakly affected by the action of the wall of porosity 0.6 (i.e. fabric with less open spaces). This fact probably helps to retard the progression and rupture of the aneurysm. The simulation result shows that the presence of a textile wall of porosity 0.6 reduced the disturbed and recirculated flow, which means fewer stagnant regions.

As a result, the maximum flow velocity at the maximum aneurysm diameter was 17.85 percent higher with the presence of the textile wall of porosity 0.6 and closer to the core flow as compared to the textile wall of porosity 1.0, Fig. 4.3.7 and 4.3.6. This difference between both cases can be explained by the fact that the recirculating vortex produces complicated local conditions and energy losses probably occur due to friction with the wall.

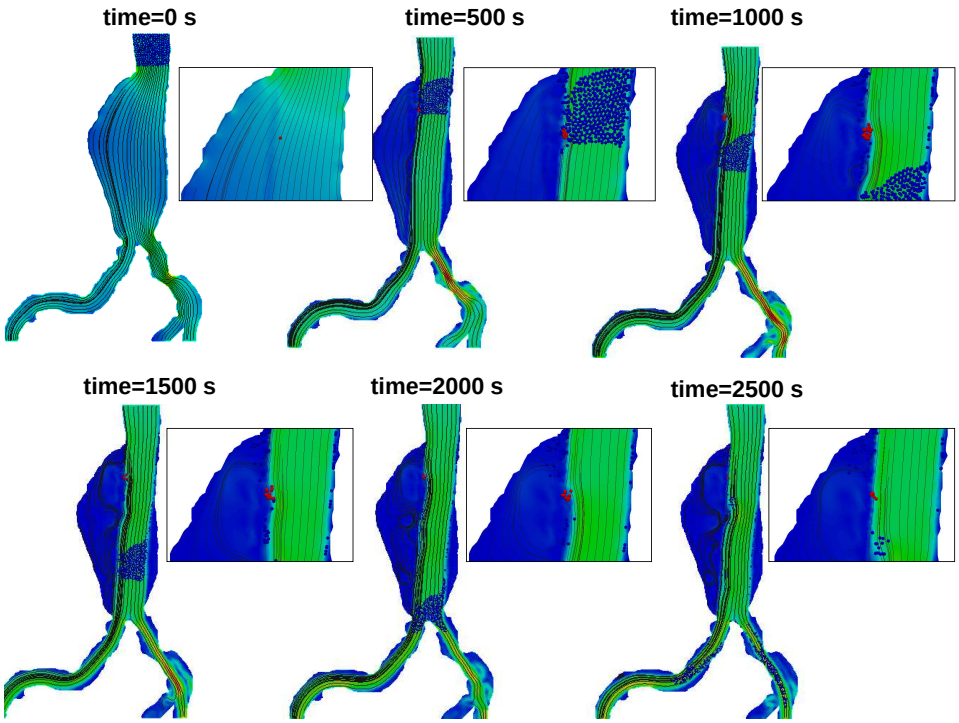

Figure 4.3.6: Infrarenal aneurysm based on an MRA image: distribution of particles and flow for different time instants. The porosity of the textile wall has a value of 0.6 (i.e.. fabric with less open spaces). Platelet aggregation is initiated by placing one active platelet attached to the textile wall near the proximal neck. The color shows the velocity magnitude in m/s.

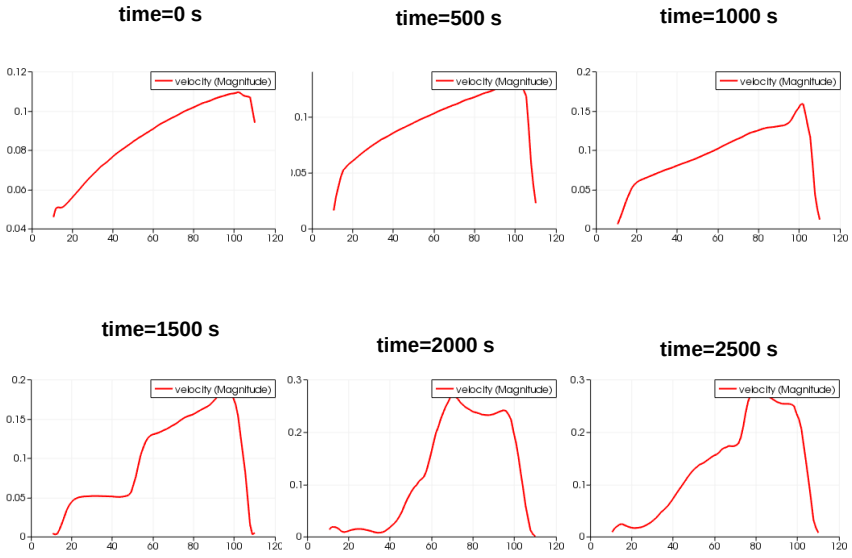

Figure 4.3.7: Velocity profiles (velocity magnitude in m/s) in the maximum aneurysm diameter for different time instants. The porosity of the textile wall has a value of 1.0 (i.e.. open fabric).

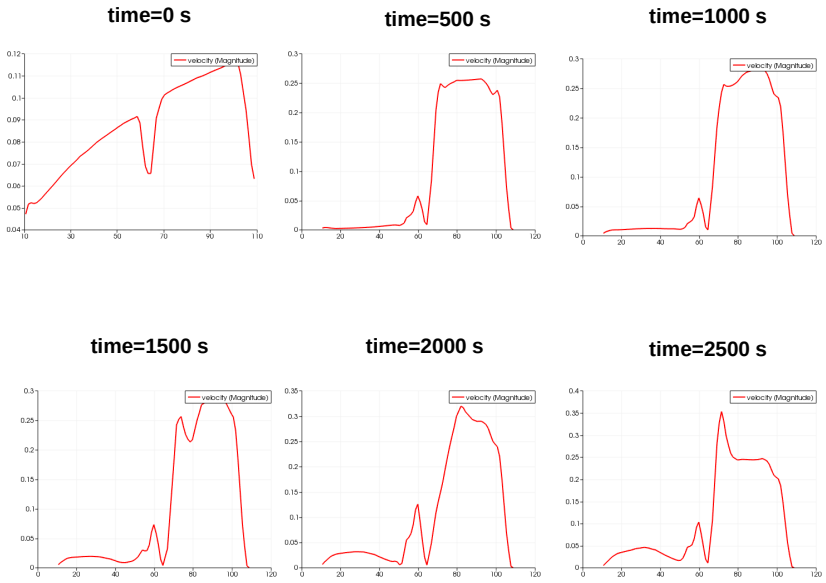

Figure 4.3.8: Velocity profiles (velocity magnitude in m/s) in the maximum aneurysm diameter for different time instants. The porosity of the textile wall has a value of 0.6 (i.e.. fabric with less open spaces).

Figure 4.3.9 shows the number of platelets adhered to the textile vascular wall at a infrarenal aneurysm. The plot revealed that the growth rate was initially higher when the porosity was reduced, but it quickly collapsed and the final size of the thrombus became smaller compared to the textile wall of 1.0. This behavior is likely due to the fact that the high velocities acting on the particles limit the growth of the thrombus.

Lastly, a large recirculating flow region results in large residence time, which could be a contributing factor for thrombosis in the aneurismal cavity. Once trapped the particles in the recirculation zone, they experience a prolonged contact, promoting adhesion and aggregation to the wall. The case with an open fabric, a PRI of 89.86 percent was observed after 1500s, while a PRI of 22.32 percent was observed with the textile wall of porosity 0.6, Fig.4.3.10.

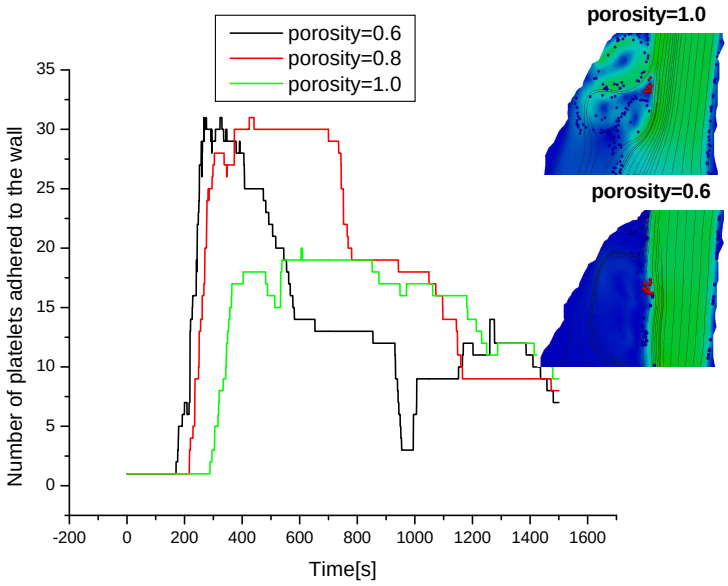

Figure 4.3.9: Number of platelets adhered to the textile wall at a infrarenal aneurysm. The results are shown with different porosities of the textile wall and it revealed that the growth rate was initially higher when the porosity was reduced, but it quickly collapsed and the final size of the thrombus became smaller compared to the textile wall of 1.0.

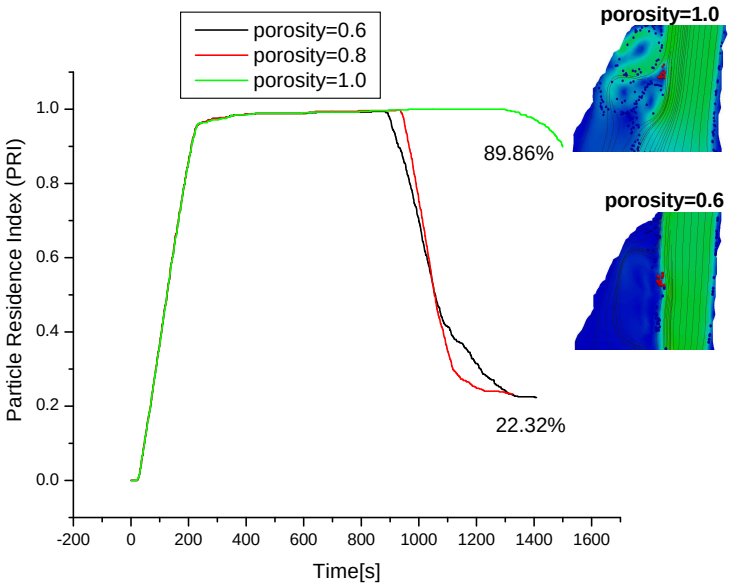

Figure 4.3.10: Time evolution of PRI in the infrarenal aneurysm zone. The PRI for this case was defined as the ratio of the number of particles inside the aneurysm zone divided by the total number of initially released particles. A PRI of 89.86 percent was observed for the open fabric (porosity=1.0) after 1500s, while a PRI of 22.32 percent was observed with the wall of porosity 0.6.

Chapter 5

CONCLUSIONS, CONTRIBUTION AND FUTURE WORK

5.1 Conclusions

The flow pattern and fluid-particle interaction of individual particles with platelet-like properties have been described in textile vascular grafts with an anastomoses of end-to-end configuration, for both macroscopic and microscopic viewpoints. The effect of two different types of fabrics, electrospun and woven, was evaluated at several length scales considering the pass of fluid and the transport of particles through the porous walls. The results have shown that the type of fabric in textile vascular grafts and the degree of porosity and permeability affect the local fluid dynamics and the level of penetration of platelet particles through the graft wall, thus indicating their importance as design parameters.

It was found during the simulations that the variability of permeability strongly depends on the micro-structure of the fabric, changing the local dynamics of fluid and the time of residence of platelets inside the wall. For instance, although the electrospun sample had higher porosity values than the woven sample, its micro-structure was more complex, causing lower permeability values, higher PRI values, and increasing the likelihood that the platelets be aggregated and deposited within the wall. Furthermore,the micro-scale permeability and porosity were input for flow simulations on the macro-scale. The variation on the micro-scale has an important influence on the macro-scale. It is important that these variations be captured in a sufficiently accurate way, in order to be able to perform reliable macro-scale simulations.

From macroscopic viewpoint, the presence of a porous wall along a duct causes deviations from Poiseuille flow due to leakage flow through the wall. The axial flow rate and the shear stress are reduced in magnitude as the permeability is increased and this behavior is even observed for different diameters and porosities. Moreover, with leakage flow through the porous wall, the particles move to the wall, increasing the residence time.

It was possible to observe that the textile wall with different porosities, acts like a barrier between the blood and the aneurysm zone, which affects the flow pattern, the number of platelets adhered to the artificial surface and the time of residence of platelets inside the aneurysm zone. It was identified that the thrombus formation has a large impact on the flow field, defining a stagnation point and dividing streamlines which pass through this point. The simulation results also show that the presence of a textile wall of porosity 0.6 reduces the recirculating flow, reduces PRI in the aneurysm zone and limits the growth of the thrombus, compared to the textile wall of porosity 1.0.

Lastly, the multi-scale method (combining Finite Element Method for fluid flow and Molecular Dynamic for discrete particles) is particularly attractive for modeling blood flow and cellular response in textile vascular grafts, providing an insight both on local hemodynamics at macro level and on interaction between platelets at a micro level.

In conclusion, the development of new textile grafts may be improved if details of the flow pattern and the mobility of blood cells through the graft wall are known and predictable, before the graft is manufactured.

5.2 Contribution

The contributions to this dissertation are:

- The development of a multiscale mathematical model that represent the behavior of local fluid dynamics and the fluid-particle interaction of platelets, considering the presence of the textile wall (porous media).
- The development of a code that couples the Finite Element Method (FEM) and a Particle Method , including one, two and four-way coupling for fluid-particle interaction and a fictitious domain model that represents the no-slip boundary condition between the free-fluid and the textile wall.
- A numerical study that quantify the influence of the type of fabric, permeability and porosity of textile vascular grafts at several scales of length, both on local fluid dynamics and on the fluid-particle interaction among platelets.

The majority of computational studies of vascular grafts have focused exclusively on the flow pattern at a macro level without considering the presence of the textile wall. In general, the blood is treated as a homogeneous fluid. However, they do not consider the effect of the fabric type, its permeability and its porosity, on local fluid dynamics at several scales of length. Also, they do not simultaneously consider the plasma flow as well as the motion of individual platelets, related with clot formation, reduction of flow and graft occlusion. Hence, this work could represent a

contribution to the titanic task of trying to improve the design of textile vascular grafts in end-to-end configurations, indicating the importance of these design parameters on mass transport and normal hemostasis after implantation.

5.3 Future Work

Although the proposed model seems to be useful in evaluating the macro and micro-flow patterns and the fluid-particle interaction among platelets considering the types of fabric of a textile graft, an important future work would be: to extend the work to other type of textile vascular grafts and topologies, to extend the simulations from two to three dimensional analysis for the AAA case with the presence of a textile vascular graft, and experimental tests to evaluate and validate how the porosity and permeability change over time due to the penetration and deposition of cells like platelets, endothelials and fibroblasts (see Appendix B). With these developments, the proposed work would contribute with more details to the understanding of this research.

Appendix A

The Method of Characteristic-Galerkin

The Characteristic-Galerkin method evaluates the time derivative of a vector field on Lagrangian frame, following the trajectory of a material point of the mesh through its characteristic curve, finding the position where the point was an instant of time before [70, 34]. The material derivative is the starting point to perform the temporal discretization process in this method.

Consider the total acceleration in the Navier-Stokes:

$$\frac{\partial \mathbf{u}}{\partial t} + \mathbf{u} \cdot \nabla \mathbf{u} \tag{A.0.1}$$

This side can be discretized as $D\mathbf{u}/Dt$ where D is the material derivative which can be discretized by an implicit method in a Finite Difference method scheme:

$$\frac{D\mathbf{u}}{Dt} = \frac{\mathbf{u}^{n+1}(\mathbf{x}) - \mathbf{u}^{n}(\mathbf{X}^{n}(\mathbf{x}))}{\triangle t^{n}} \tag{A.0.2}$$

where $\mathbf{X}^{n}(\mathbf{x})$ is an approximation of the solution at $\tau = n\triangle t$ of the ordinary differential equation:

$$\frac{d\mathbf{X}}{d\tau} = \mathbf{u}(\mathbf{X}, \tau) \qquad \mathbf{X}((n+1)\triangle t) = \mathbf{x} \tag{A.0.3}$$

The trajectory of a material point of the domain is done by Backward Euler scheme:

$$\mathbf{X}^{n} = \mathbf{x} - \mathbf{u}^{n}(\mathbf{x})\triangle t \tag{A.0.4}$$

where $\mathbf{X}^{n}$ is the position where the particle was an instant before, $\mathbf{x}$ is the position on the grid, and $\mathbf{u}^{n}(\mathbf{x})$ is the velocity evaluated on the grid.

Keeping the Finite Element method in mind , the problem becomes:

$$\int_{\Omega} \frac{D\mathbf{u}}{Dt}\mathbf{v}d\Omega = \int_{\Omega} \frac{1}{dt}\mathbf{u}^{n+1}\mathbf{v}d\Omega - \int_{\Omega} \frac{1}{dt}\mathbf{u}^{n}(\mathbf{X}^{n})\mathbf{v}d\Omega \tag{A.0.5}$$

Appendix B

Progress of Future Work

The aim of this study is to evaluate the effect of thickness and cellular deposition with fibroblasts in the permeability and porosity of electrospun samples. Electrospun samples of polyurethane (PUR) are been manufactured with the electrospinning technique. Once the samples are obtained, cardiac fibroblasts are cultured for an incubation period of 48, 96, 192 and 240 hours. Then, porosity and permeability are measured according to ISO7198 international standard. Lastly, cell proliferation is analyzed by optical techniques. A summary of the process is presented in Fig. B.0.1.

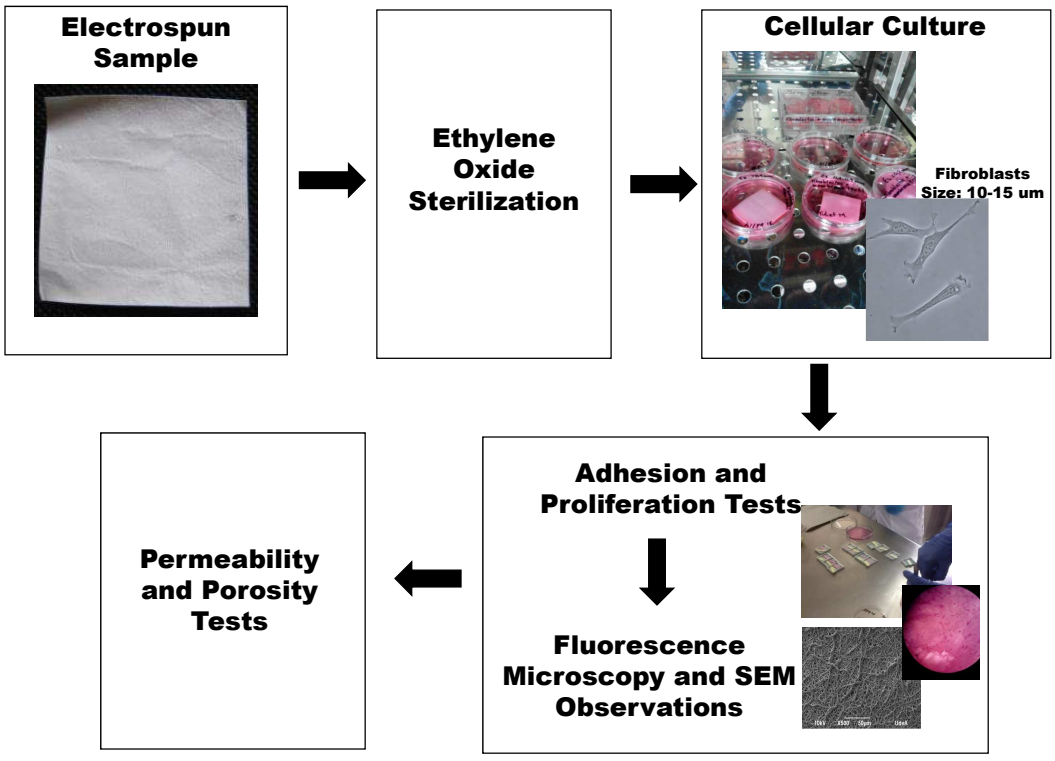

Figure B.0.1: Study of the effect of thickness and cellular deposition with fibroblasts in the permeability and porosity of electrospun samples.

Appendix C

Properties of blood constituents, vessels dimensions and hemodynamics values of the aorta

Human blood is a concentrated suspension of cells in a complex aqueous solution [25]. Various types and shapes of cells are immersed in plasma, which displays Newtonian characteristics. Some properties of blood constituents are summarized in Table C.1:

Table C.1: Properties of blood constituents. [25]

Material	Red blood cell	Platelet	Leukoytes	Plasma	Whole blood
Density $[g/cm^3]$	1.09	1.069	1.07-1.09	1.03	1.054
Viscosity $dyn \cdot s/cm^2]$	-	-	-	0.014	0.0309
Blood cell count $[\#/cm^3]$	5×10^9	3×10^8	7.0×10^6	-	-
Volume $[\mu m^3]$	88	5.17	460	-	-
Size $[\mu m]$	7.7 x 2.8	3.0	9.5	-	-

On the other hand, there are a wide length scale range in the cardiovascular system [22]. Blood vessel dimensions range from the order of 25 mm to 30 mm for large-scale flows (e.g., aorta) to length scales of a few microns for small-scale flows (e.g., capillaries). Some blood vessel dimensions are listed in Table C.2.

Table C.2: Blood vessel dimensions [22].

Vessel	Mean Wall Thickness [mm]	Mean Diameter [mm]
Artery	25	1
Arteriole	0.03	0.006
Capillary	0.008	0.0005
Venule	0.02	0.001
Vein	5	0.5

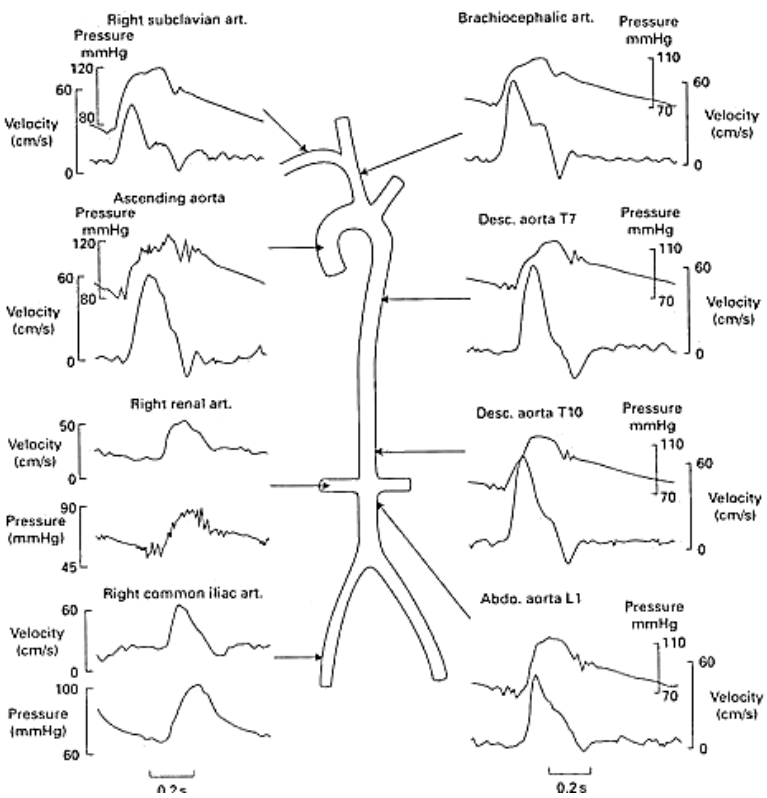

Figure C.0.1: Arterial pressures and flow rates of the human aorta [84].

Lastly, for the numerical case of the Abdominal Aortic Aneurysms (AAA) model, hemodynamics values of the aorta were taken from [84], see Fig. C.0.1.

Bibliography

[1] FreeFem++. http://www.ann.jussieu.fr/lehyaric/ffcs/.

[2] ImageJ: Image Processing and Analysis in Java. http://imagej.nih.gov/ij/index.html.

[3] International Standard ISO 7198. Cardiovascular implants-tubular vascular prostheses.

[4] ScotCad Textiles Ltda: http://www.scotweave.com/.

[5] Techtext cad. http://www.tensiontech.com.

[6] TexEng-Weave Engineer.http://softwaresolutions.fibre2fashion.com/company/texeng.

[7] Nektar++: An efficient h to p finite element framework. http://www.nektar.info/, 2013.

[8] Particle Finite Element (PFEM). http://www.cimne.com/pfem/, July 2014.

[9] ABDESSALEM, B., AND DURAND, B. Blood flow in a polyester textile vascular prosthesis: experimental and numerical study. *Textile Research Journal 71*, 2 (2001), 178–183.

[10] ABDESSALEM, B., DURAND, B., AKESBI, S., CHAKFE, N., AND KRETZ, J. Fluid-structure interaction in a free end textile vascular prosthesis. *The European Physical Journal Applied Physics 31* (2005), 211–216.

[11] ABDESSALEM, B., DURAND, B., AKESBI, S., CHAKFE, N., AND KRETZ, J. Numerical simulation of blood flow in a curved textile vascular prosthesis. *Journal of Textile Institute 96* (2005), 117–122.

[12] ALMOMANI, T., UDAYKUMAR, H., MARSHALL, J., AND CHANDRAN, K. Micro-scale dynamic simulation of erythrocyte platelet interaction in blood flow. *Annals of Biomedical Engineering 36*, 6 (Jun 2008), 905–920.

[13] ANGOT, P., BRUNEAU, C., AND FABRIE, P. A penalization method to take into account obstacles in incompressible viscous flows. *Numerische Mathematik 81*, 4 (1999), 497–520.

[14] BARTELS, V. *Handbook of Medical Textiles*. Woodhead Publishing in association with The Textile Institute, 2011.

[15] BELOV, E., LOMOV, S., VERPOEST, I., PETERS, T., ROOSE, D., PARNAS, R., HOES, K., AND SOL, H. Modelling of permeability of textile reinforcements: lattice boltzmann method. *Composites Science and Technology 64* (2004), 1069 – 1080.

[16] BERGMEISTER, H., STROBL, M., GRASL, C., LISKA, R., AND SCHIMA, H. Tissue engineering of vascular grafts. *European Surgery 45*, 4 (2013), 187–193.

[17] BERTHIER, J., AND SILBERZAN, P. *Microfluidics for biotechnology. Second Edition.* Artech House, 2010.

[18] BETANCUR, E. A two step optimization process using freefem++: topology optimization. Tech. rep., Mecanica Aplicada. Universidad Eafit., 2013.

[19] BRONZINO, J. *The Biomedical Engineering. Handobook.*, vol. Second. CRC Press, Springer, IEEE Press, 2000.

[20] BUCHANAN, C., VOIGHT, E., SZOT, C., FREEMAN, J., VLACHOS, P., AND RYLANDER, M. Three-dimensional microfluidic collagen hydrogels for investigating flow-mediated tumor-endothelial signaling and vascular organization. *Tissue Eng Part C Methods 20*, 1 (Jan 2013), 64–75.

[21] CHANDRAN, K. Role of computational simulations in heart valve dynamics and design of valvular prostheses. *Cardiovasc Eng Technol 1*, 1 (March 2010), 18–38.

[22] CHANDRAN, K. B. *Biofluid Mechanics. The Human Circulation*. CRC Press. 451 pages, 2007.

[23] CHLUPAC, J., FILOVA, E., AND BACAKOVA, L. Blood vessel replacement: 50 years of development and tissue engineering paradigms in vascular surgery. *Physiol. Res 58*, 2 (October 2009), 119–139.

[24] CIOFFI, M., BOSCHETTI, F., RAIMONDI, M., AND DUBINI, G. Modeling evaluation of the fluid-dynamic microenvironment in tissue-engineered constructs: a micro-ct based model. *Biotechnol Bioeng. 93*, 3 (Feb 2006), 500–510.

[25] CLEMENT, K. *Biofluid Dynamics. Principles and selected applications*. Taylor and Francis Group, 2006.

[26] COMSOL. Coupled free and porous media flow. http://www.comsol.com, October 2012.

[27] CONNELL, B., MCGLOUGHLIN, T., AND WALSH, M. Factors that affect mass transport from drug eluting stents into the artery wall. *Biomedical Engineering Online 9* (2010), 15.

[28] CONTRERAS, C. Behavior of engineered nanoparticles in aqueous solutions and porous media: connecting experimentation to probabilistic analysis. Master's thesis, The University of Texas at San Antonio, 2011.

[29] CONTRO, R., AND VENA, P. Computational models for biological tissues and biomedical implants. *Engineering Computations 20*, 5-6 (2003), 513–523.

[30] CURTIN, W. A., AND MILLER, R. E. Atomistic/continuum coupling in computational materials science. *Modelling and Simulation in Materials Science and Engineering 11*, 3 (2003), R33.

[31] DIAS, M., FERNANDEZ, P., GUDES, J., AND HOLLISTER, S. Permeability analysis of scaffolds for bone tissue engineering. *J. of Biomechanics 45* (2012), 938–944.

[32] DIEVAL, F., CHAKFE, N., BIZONNE, S., MAGNEN, J. L., BEAUFIGEAU, M., MATHIEU, D., RIEPE, G., KRETZ, J., AND DURAND, B. Les tests mechaniques devaluation des protheses vasculaires. *ITBM-RBM Elsevier 22* (2001), 70–87.

[33] DOBRICH, O., GEREKE, T., AND CHERIF, C. Modelling of textile composite reinforcements on the micro-scale. *Autex Research Journal 14*, 1 (March 2014), 28–33.

[34] DONEA, J., AND HUERTA, A. *Finite Element Methods for Flow Problems*, third ed. Wiley, 2003.

[35] EHRHARDT, M. An introduction to fluid-porous interface coupling. *Progress in Computational Physics : "Coupled Fluid Flow in Energy, Biology and Environmental Research" 2*, 10 (2010), 3–12.

[36] FDA. Guidance for Industry and FDA Staff: Guidance Document for Vascular Prostheses 510(k) Submissions. http://www.fda.gov/medicaldevices, May 2012.

[37] FILIPOVIC, N., KOJIC, M., AND TSUDA, A. Modeling thrombosis using dissipative particle dynamics method. *Philosophical Transactions of the Royal Society of London 366*, 1879 (2008), 3265–3279.

[38] FOR VASCULAR SURGERY, V. S. Abdominal aortic aneurysm.

[39] GALINDO, C., LIMA, C., CARDOSO, J., GALINDO, G., COSTA, V., AND PENHA, F. Isolated atherosclerotic aneurysm of the superficial femoral artery - case report. *J Vasc Br 2*, 2 (2003), 145–147.

[40] GAO, F., UEDA, H., LI, G., AND OKADA, H. Fluid structure interaction simulation in three-layered aortic aneurysm model under pulsatile flow: comparison of wrapping and stenting. *Journal of Biomechanics 46* (February 2013), 1335–1342.

[41] GARCIA J, GONZALEZ, B. J. Simulation and analysis of flow in different geometrical arrays of a vascular graft. *Universidad de los Andes* (2013).

[42] GIORDANA, S., SHERWIN, S., PEIRO, J., DOORLY, D., CRANE, J., LEE, K., CHESHIRE, N., AND CARO, C. Local and global geometric influence on steady flow in distal anastomoses of peripheral by-pass grafts. *J Biomech Eng 127*, 7 (December 2005), 1087–1098.

[43] GLOWINSKI, R., PAN, T., HESLA, T., AND JOSEPH, D. A distributed lagrange multiplier/fictitious domain method for particulate flows. *International Journal of Multiphase Flow 25*, 5 (1999), 755 – 794.

[44] GORE. Three trusted technologies-one of a kind graft. http://www.goremedical.com/hybrid/, July 2012.

[45] GREENHALGH, E., AND DUNN, M. Modeling blood flow through vascular grafts. Tech. rep., Philadelphia College of Textile and Science, 1998.

[46] GRINBERG, L., MOROZOV, V., FEDOSOV, D., INSLEY, J., PAPKA, M., KUMARAN, K., AND KARNIADAKIS, G. A new computational paradigm in multiscale simulations: Application to brain blood flow. In *High Performance Computing, Networking, Storage and Analysis (SC)* (Seatle, WA, Nov 2011), Proceedings of 2011 International Conference for High Performance Computing, Networking, Storage and Analysis (SC '11), IEEE, pp. 1–12.

[47] HASAN, A., MEMIC, A., ANNABI, N., HOSSAIN, M., PAUL, A., DOKMECI, M., DEHGHANI, F., AND KHADEMHOSSEINI, A. Electrospun scaffolds for tissue engineering of vascular grafts. *Acta Biomateria 10* (2014), 11–25.

[48] KAMADA, H., TSUBOTA, K., NAKAMURA, M., WADA, S., ISHIKAWA, T., AND YAMAGUCHI, T. A three-dimensional particle simulation of the formation and collapse of a primary thrombus. *International Journal for Numerical Methods in Biomedical Engineering 26*, 3-4 (2010), 488–500.

[49] KHADRA, K., ANGOT, P., PARNEIX, S., AND CALTAGIRONE, J. Fictitious domain approach for numerical modelling of navier stokes equations. *International Journal for Numerical Methods in Fluids 34*, 8 (December 2000), 651–684.

[50] KOJIC, M., FILIPOVIC, N., AND TSUDA, A. A mesoscopic bridging scale method for fluids and coupling dissipative particle dynamics with continuum finite element method. *Computer Methods in Applied Mechanics and Engineering 197* (2008), 821 – 833.

[51] KOJIC, M., FILIPOVIE, N., STOJANOVI, B., AND KOJIC, N. *Computer modeling in bioengineering. Theoretical background, examples and software*. John Wiley and Sons, Ltd, 2008.

[52] KU LEUVEN. Wisetex suit. https://www.mtm.kuleuven.be/onderzoek/composites/software/wisetex, 2012.

[53] KUTZ, M. *Standard Handbook Biomedical Engineering and Design. Chapter 20: Cardiovascular Devices*. McGRAW-HILL, 2003.

[54] LEI, M., ARCHIE, J., AND KLEINSTREUER, C. Computational design of a bypass graft that minimizes wall shear stress gradients in the region of the distal anastomosis. *Journal of Vascular Surgery 25*, 4 (1997), 637–646.

[55] LEISEN, J., BECKHAM, H., AND FARBER, P. Microflow in textiles. Tech. rep., National Textile Center. Annual report, 2007.

[56] LEONG, E. Vascular graft. 9th HKL Vascular Surgery Seminar 2010.

[57] LEUPRECHT, A., PERKTOLD, K., PROSI, M., BERK, T., TRUBEL, W., AND SCHIMA, H. Numerical study of hemodynamics and wall mechanics in distal end-to-side anastomoses of bypass grafts. *Journal of Biomechanics 35, Issue 2* (2002), 225–236.

[58] LI, X., POPEL, A., AND KARNIADAKIS, G. Blood plasma separation in y-shaped bifurcating microfluidic channels: a dissipative particle dynamics simulation study. *Physical Biology 9* (2012), 1–12.

[59] LIU, G. R., AND LIU, M. B. *Smoothed Particle Hydrodynamics: A Meshfree Particle Method*. World Scientific, 2006.

[60] LONGEST, P., KLEINSTREUER, C., AND DEANDA, D. Numerical simulation of wall shear stress and particle-based hemodynamic parameters in pre-cuffed and streamlined end-to-side anastomoses. *Annals of Biomedical Engineering 33*, 12 (2005), 1752–1766.

[61] LOTH, F., FISCHER, P. F., AND BASSIOUNY, H. S. Blood flow in end-to-side anastomoses. *Annual Review of Fluid Mechanics 40* (2008), 367–393.

[62] MANKODI, H. Application of textile materials in cardiovascular implants. http://www.fibre2fashion.com/industry-article/2/140/application-of-textile-materials1.asp, 2012.

[63] NABOVATI, A., LLEWELLIN, E. W., AND SOUSA, A. C. A general model for the permeability of fibrous porous media based on fluid flow simulations using the lattice boltzmann method. *Composites Part A: Applied Science and Manufacturing 40* (2009), 860 – 869.

[64] NABOVATI, A., LLEWELLIN, E. W., AND SOUSA, A. C. Through-thickness permeability prediction of three-dimensional multifilament woven fabrics. *Composites Part A: Applied Science and Manufacturing 41* (2010), 453 – 463.

[65] NAITO, Y., SHINOKA, T., DUNCAN, D., HIBINO, N., SOLOMON, D., CLEARY, M., RATHORE, A., FEIN, C., CHURCH, S., AND BREUER, C. Vascular tissue engineering: Towards the next generation vascular grafts. *Advanced Drug Delivery Reviews 63* (2011), 312 – 323.

[66] NGO, N., AND TAMMA, K. Microscale permeability predictions of porous fibrous media. *International Journal of Heat and Mass Transfer 44*, 16 (2001), 3135 – 3145.

[67] ONATE, E., CELIGUETA, M., LATORRE, S., CASAS, G., ROSSI, R., AND ROJEK, J. Lagrangian analysis of multiscale particulate fflow with the particle finite element method. *Computational Particle Mechanics 1*, 1 (May 2014), 85–102.

[68] PAPAHARILAOU, Y., DOORLY, D., AND SHERWIN, S. The influence of out-to-plane geometry on pulsatile flow within a distal end-to-side anastomoses. *Journal of Biomechanics 35* (2002), 1225–1239.

[69] PAPAIOANNOU, T., AND STEFANADIS, C. Vascular wall shear stress: basic principles and methods. *Hellenic Journal of Cardiology 46*, 1 (2005), 9–15.

[70] PIRONNEAU, O. On the transport-diffusion algorithm and its applications to the navier-stokes equations. *Numerische Mathematik 38* (1982), 309–332.

[71] PIVKIN, I., RICHARDSON, P., AND KARNIADAKIS, G. Effect of red blood cells on platelet aggregation. *Engineering in Medicine and Biology Magazine. IEEE 28.2* (2009), 32–37.

[72] PIVKIN, I. V., RICHARDSON, P. D., AND KARNIADAKIS, G. Blood flow velocity effects and role of activation delay time on growth and form of platelet thrombi. *Proceedings of the National Academy of Sciences 103*, 46 (2006), 17164–17169.

[73] PMI PUBLICATIONS. Characterization of pore structure. http://www.pmiapp.com/publications.html, July 2012.

[74] PRINCE, M. R. Gadolinium-enhanced magnetic resonance angiography of abdominal aortic aneurysms. *Journal of Vascular Surgery 21, Issue 4* (1995), 656–669.

[75] PROBST, M., LULFESMANN, M., NICOLAI, M., BUCKER, H., BEHR, M., AND BISCHOF, C. Sensitivity of optimal shapes of artificial grafts with respect to flow parameters. *Computer Methods in Applied Mechanics and Engineering 199*, 17-20 (2010), 997 – 1005.

[76] ROJEK, J., AND ONATE, E. Multiscale analysis using a coupled discrete/finite element model. *Interaction and Multiscale Mechanics 1*, 1 (2007), 1–31.

[77] SANDIA NATIONAL LABORATORIES. LAMMPS Molecular Dynamics Simulator.http://lammps.sandia.gov, 2014.

[78] SANDOR, I., BERNAD, E., CRAINA, M., SARGAN, I., TOTORAN, A., AND COSMIN, B. Particle deposition and related hemodynamic parameters in the multiple stenosed right coronary artery. *Clin. Med. Res. 4*, 3 (2012), 177–189.

[79] SCHOEPHOERSTER, R., OYNES, F., NUNEZ, G., KAPADVANJWALA, M., AND DEWANJEE, M. Effects of local geometry and fluid dynamics on regional platelet deposition on artificial surfaces. *Arteriosclerosis and Thrombosis: a journal of vascular biology 13*, 12 (Dec 1993), 1806–1813.

[80] SCOTTI, C., SHKOLNIK, A., MULUK, S., AND FINOL, E. Fluid-structure interaction in abdominal aortic aneurysms: effects of asymmetry and wall thickness. *Biomedical Engineering Online 4*, 64 (2005), 1–22.

[81] TANG, S., HOU, T. Y., AND LIU, W. K. A mathematical framework of the bridging scale method. *International Journal for Numerical Methods in Engineering 65*, 10 (2006), 1688–1713.

[82] TANI, K. Earth Simulator Project in Japan. *High Performance Computing 1940*, 2000 (Apr 2000), 33–42.

[83] TAYLOR, C., AND HUMPHREY, J. Open problems in computational vascular biomechanics: Hemodynamics and arterial wall mechanics. *Computer Methods in Applied Mechanics and Engineering 198*, 45 (2009), 3514 – 3523.

[84] TAYLOR, D. *Blood flow in arteries*, second ed. Wiley Online Library, London, 1974.

[85] TSUBOTA, K., WADA, S., KAMADA, H., KITAGAWA, Y., LIMA, R., AND YAMAGUCHI, T. A particle method for blood flow simulation: Application to flowing red blood cells and platelets. *Journal of the Earth Simulator 5* (Mar 2006), 2–7.

[86] TU, J., INTHAVONG, K., AND AHMADI, G. *Computational Fluid and Particle Dynamics in the Human Respiratory System*. Springer, 2013.

[87] TURA, A. *Vascular Grafts. Experiment and Modelling*. WIT Press, 2003.

[88] VAFAI, K. *Porous media: Application in biological systems and biotechnology*. CRC Press, 2011.

[89] VALLIER, A. Tutorial icolagrangianfoam/solidparticle. Tech. rep., CFD with opensource software OpenFoam, 2010.

[90] VEIT, D., Ed. *Simulation in Textile Technology. Theory and applications*. Woodhead Publishing in association with The Textile Institute, 2012.

[91] VERLEYE, B., CROCE, R., GRIEBEL, M., KLITZ, M., LOMOV, S., MORREN, G., SOL, H., VERPOEST, I., AND ROOSE, D. Permeability of textile reinforcements: Simulation, influence of shear and validation. *Composites Science and Technology 68*, 13 (2008), 2804 – 2810.

[92] VERLEYE, B., MORREN, G., LOMOV, S., SOL, H., VERPOEST, I., AND ROOSE, D. User-friendly permeability predicting software for technical textiles. *Research Journal of Textile and Apparel 13*, 2 (May 2009), 19–27.

[93] WANG, Y. Fabric Mechanics.http://www.fabricmechanics.com, 2012.

[94] YAMAGUCHI, T., ISHIKAWA, T., IMAI, Y., MATSUKI, N., XENOS, M., DENG, Y., AND BLUESTEIN, D. Particle-based methods for multiscale modeling of blood flow in the circulation and in devices: Challenges and future directions. *Ann Biomed Eng. 38*, 3 (Mar 2010), 1225–1235.

[95] YANG, C., DING, Y., YORK, D., AND BROECKX, W. Numerical simulation of sedimentation of microparticles using the discrete particle method. *Particuology 6*, 2008 (2008), 38 – 49.

[96] YU, Z., AND SHAO, X. Direct numerical simulation of particulate fflow with fictitious domain method. *Internation Journal of Multiphase Flow 36* (2010), 127–134.

[97] ZILLA, P., BEZUIDENHOUT, D., AND HUMAN, P. Prosthetic vascular grafts: Wrong models, wrong questions and no healing. *Biomaterials 28*, 34 (2007), 5009 – 5027.